

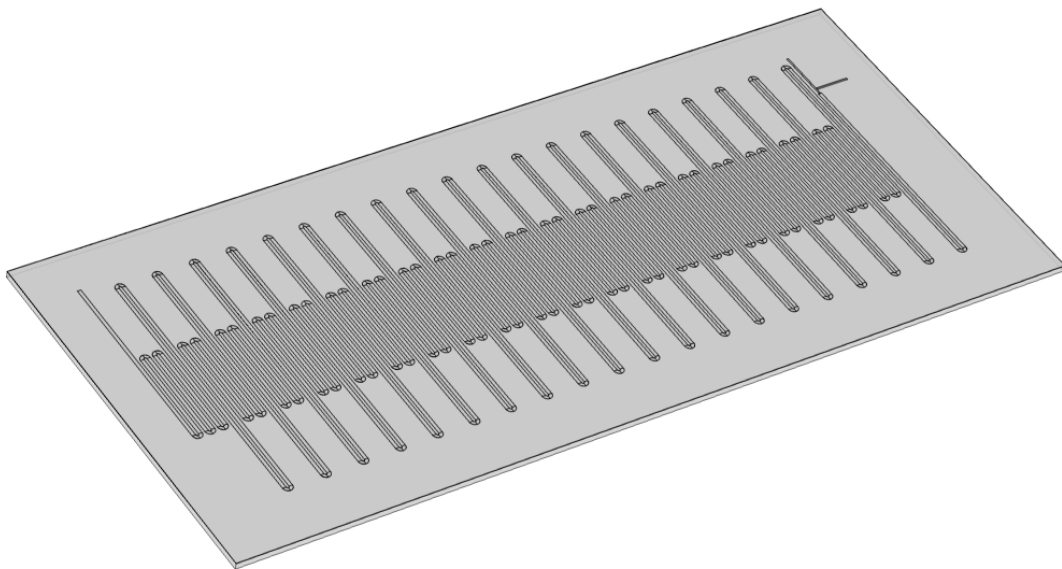
4<sup>TH</sup> SEMESTER

---

# DESIGN AND FABRICATION OF MICROFLUIDIC PCR CHIPS

---

13th of October 2025



Nanobiotechnology, 5.321  
Department of Materials and Production, Aalborg University





**AALBORG UNIVERSITY**  
STUDENT REPORT

**Aalborg University**

Nanotechnology

Skjernvej 4A

Aalborg

**Title:**

Design and fabrication of microfluidic PCR chips

**Semester:**

4<sup>th</sup> semester

**Project period:**

1st of September 2024– 13th of October 2025

**Project group:**

5.321

**Email:**

bballa23@student.aau.dk

**Supervisors:**

Evamaria Petersen

Leonid Gourevitch

**Number of pages:**

46

**Number of appendix pages:**

2

**Finish date:**

13th of October 2025

**Abstract:**

Continuous-flow PCR systems are known to decrease the thermal mass compared to conventional thermocyclers by maintaining constant temperature zones. This results in faster PCR completion while limiting reagent consumption. These methods are easily inhibited by the adsorption of PCR components due to their large surface-to-volume ratios. Droplet-based PCR circumvents this by eliminating the contact between the sample and the device's surface. In this paper, the design and fabrication of a continuous-flow fixed-loop droplet-based PCR on a chip, which is capable of 25 cycles, were investigated. The chip was fabricated by etching microfluidic channels into silicon with a T-junction integrated into the design. The channels of the chip were capped off with a PDMS coverplate. The heat distribution of the device was first simulated. Stable temperature regions were generated using one resistive heater and one Peltier heater on two edges of the chip. Copper blocks were used to further define the regions by using two heating elements to define the annealing and denaturation zones, while relying on the gradient formed by heat exchange to form the extension zone. The device is capable of generating stable and uniform droplets. The PCR product of the chip was found to be shorter than expected.

## Resumé:

Mikrofluidiske PCR-systemer er kendt for at reducere den termiske masse sammenlignet med konventionelle termocyclere ved at opretholde konstante temperaturzoner. Dette resulterer i hurtigere PCR-gennemførelse og begrænser samtidig reagensforbruget. Disse metoder hæmmes let af adsorptionen af PCR-komponenter på grund af deres store overflade-til-volumen-forhold. Dråbebaseret PCR omgår dette ved at eliminere kontakten mellem prøven og enhedens overflade. I denne artikel undersøges designet og fremstillingen af en mikrofluidiske fastsløjfe dråbebaseret PCR på en chip, der er i stand til at udføre 25 cyklusser. Chippen blev fremstillet ved at ætse mikrofluidiske kanaler i silicium med en T-forbindelse integreret i designet. Chipens kanaler blev afdækket med en PDMS-dækplade. Enhedens varmefordeling blev først simuleret. Der blev genereret stabile temperaturområder ved hjælp af en resistiv varmeelement og et Peltier-varmeelement på to kanter af chippen. Kobberblokke blev brugt til yderligere at definere områderne ved hjælp af to varmeelementer til at definere annealing- og denatureringszonerne, mens man benyttede den gradient, der dannedes ved varmeudveksling, til at danne forlængelseszonen. Enheden er i stand til at generere stabile og ensartede dråber. PCR-produktet fra chippen viste sig at være kortere end forventet.

# Preface

---

This project is written by 4<sup>th</sup>-semester master students, group 5.321, from Aalborg University. The project was supervised by associate professors Evamaria Petersen and Leonid Gurevich. The project was written in the period of September 1<sup>st</sup> 2024 to October 13<sup>th</sup> 2025. The project focuses on the design, fabrication, and testing of a continuous-flow droplet-based PCR chips. Several fabrication methods are discussed.

The citation style used in this project was the IEEE style, and all references are summarized in the bibliography. The figures through this project were named figure "X.X" [example figure 2.1] like the tables were named table "X.X" [example table 2.1] and the equations "(X.X)" [example equation (2.1)].

Aalborg University, 13th of October 2025.

---

Zita Szegletes

---

Boldizsár Ballay

# Contents

---

<b>1</b>	<b>Introduction</b>	<b>1</b>
1.1	Polimerase Chain Reaction . . . . .	3
1.2	PCR on a Chip . . . . .	4
1.2.1	PCR Inhibition due to Adsorption . . . . .	4
1.3	Microdroplet Generation . . . . .	8
1.3.1	T-junction . . . . .	8
1.4	Lithography . . . . .	9
1.4.1	UV Lithography . . . . .	9
1.5	Dry Etching . . . . .	10
1.5.1	Bosch Process . . . . .	12
<b>2</b>	<b>Chip Design</b>	<b>14</b>
2.1	PCR chip structure . . . . .	14
2.2	Supporting Components . . . . .	16
2.2.1	Chip Holder . . . . .	16
2.2.2	Heating Elements . . . . .	16
2.2.3	Injection System . . . . .	17
<b>3</b>	<b>Methods &amp; Materials</b>	<b>19</b>
3.1	Fabrication Using Laser Ablation . . . . .	20
3.2	Fabrication Using UV Lithography and Dry Etching . . . . .	20
3.2.1	UV Lithography . . . . .	21
3.2.2	Dry Etch . . . . .	21
3.2.3	Post Processing . . . . .	21
3.3	Fabrication of Supporting Components . . . . .	22
3.3.1	Chip Holder . . . . .	22
3.3.2	Temperautre Control System . . . . .	22
3.3.3	Injection System . . . . .	22
3.4	Polymerase Chain Reaction . . . . .	23
<b>4</b>	<b>Results</b>	<b>25</b>
4.1	Laser Ablation Approach . . . . .	25
4.2	Heat Distribution Simulations . . . . .	26
4.3	Morphology of the Fabricated Chips . . . . .	30
4.3.1	Moulded PDMS Chips . . . . .	31
4.4	Qualities of the Fabricated Supporting Components . . . . .	33
4.4.1	PDMS Coverplate . . . . .	33
4.4.2	3D printed Chip Holder . . . . .	33
4.4.3	Heating System . . . . .	33
4.5	PCR on a Chip . . . . .	35
4.5.1	Droplet Generation . . . . .	35

---

4.5.2	Polymerase Chain Reaction . . . . .	35
<b>5</b>	<b>Discussion</b>	<b>39</b>
5.1	PCR on a Chip . . . . .	39
5.1.1	Future PCR on a chip experiments . . . . .	39
5.2	Heating System — Problems and Improvements . . . . .	40
5.3	Droplet Generation and Flow . . . . .	40
5.4	Optimisations and Possible Improvements . . . . .	41
5.4.1	Dead Volume . . . . .	41
5.4.2	BSA and Surfactant Concentration . . . . .	42
5.4.3	Extension Rate Optimization . . . . .	42
<b>6</b>	<b>Conclusion</b>	<b>43</b>
	<b>Bibliography</b>	<b>44</b>
.1	Appendix A . . . . .	A1
.2	Method Protocols . . . . .	A1
.2.1	UV Lithography . . . . .	A1
.2.2	Dry Etch . . . . .	A1
.2.3	Post Processing . . . . .	A1
.2.4	GeneJET Plasmid Miniprep Kit . . . . .	A1



# Introduction 1

---

Polymerase Chain Reaction, often referred to as PCR, is one of the most influential techniques in biological sciences, diagnostics, and forensic sciences. Its function, in essence, is to amplify a specific DNA fragment known as the amplicon. The discovery of the method is credited to Kary Mullis, who found that during Sanger sequencing [1], single copies of genes result in low signal levels, which they could improve by first denaturing the DNA and then redefining the amplicon using reverse primers and DNA polymerase [2]. The method was later further developed, notably with the addition of Taq polymerase from the bacteria *Thermophilus aquaticus* [3], a thermostable enzyme, which greatly simplified the process [4].

Since its discovery, many new methods have been developed, such as real-time PCR, error-prone PCR or high-throughput PCR, each further expanding upon use cases, each reducing or eliminating issues with the original method. One of the main problems with conventional PCR is its large thermal mass. It has to heat up and cool down, not only the sample, but the water bath it's in as well, which results in slow thermal cycling, making the whole process last 1-2 hours [5].

Research has shown that annealing and denaturation steps can happen under negligible amounts of time [6], which suggests that the thermal cycling can be greatly sped up. In addition, conventional PCR uses high amounts of expensive reagents, the reduction of which is of interest. This gave way to microfluidic PCR devices, also referred to as PCR-on-a-chip, or PCR chips. Generally, PCR chips can be classified as well-based PCR chips, where the sample is injected into a well, which is then heated and cooled according to thermal cycling, or as continuous-flow PCR chips, where the sample is moved through fixed temperature zones [7]. The latter has only the thermal mass of the sample, allowing for faster cycles.

The first such device was introduced by Nakano *et al.* [8], using a Teflon capillary tube as a reactor, which was wound up in a coil, then placed into a container with three oil baths, each heated to its appropriate temperature. The device is capable of 30 cycles in as little as 12 minutes, and is able to produce half of the products of a commercial thermocycler in 44 minutes [8]. These results were very promising, confirming the viability of the concept.

Capillary devices were further developed (eg. [9–11]), but the need for chip-based systems arose due to their difficulty in developing into an integrated microfluidic thermocycler. Kopp *et al.* [12] were the first to introduce a continuous-flow PCR chip in 1998. Their device was fabricated by machining a 40  $\mu\text{m}$  deep 90  $\mu\text{m}$  wide channel into glass and was capable of 20 cycles.

Developing microfluidic PCR devices poses many challenges. It is hard to maintain consistent temperature zones, which can lead to low or no yield and nonspecific amplification [5]. Another key issue is carryover contamination between samples and the adsorption of PCR components, especially of DNA polymerase [7, 13–15]. Carryover contamination may cause undesired products due to DNA adsorption to the channel walls from previous samples. The adsorption of PCR components is present in all PCR methods, but its prevalence increases in magnitude in the case of microfluidic devices, because of their large surface-to-volume ratio. The adsorption of DNA polymerase is the greatest issue, as the lower polymerase concentration both reduces yield and extension rate [13, 16].

Many methods of reducing adsorption were found, such as passive and active coatings [17], and the use of PCR in droplets [18, 19]. In droplet PCR, the sample is present as aqueous microdroplets in an oil phase. Due to the parabolic flow profile, molecules will spend different times in the system, depending on their cross-sectional location. This means that components close to the surface of the channels spend significantly more time in the chip. Single-phase PCR also suffers from the preference for short fragments and short chimeric molecules [19]. Droplet-based PCR mostly eliminates, or at least greatly reduces these problems, since the sample makes no contact with the channel walls [7, 18].

In this paper, a continuous-flow fixed-loop PCR chip with integrated microdroplet generation is designed and fabricated. Several fabrication methods are considered, including laser ablation, Polydimethylsiloxane (PDMS) moulding, and silicon etching.

## 1.1 Polymerase Chain Reaction

The Polymerase Chain Reaction (PCR) is the process of amplifying DNA molecules. The process consists of three steps: denaturation, annealing, and extension. These steps are repeated numerous times to obtain a much larger sample size. During denaturation, the temperature is increased to 95°C to break up the hydrogen bonds between the sense and antisense strands of the dsDNA. Upon denaturation, the temperature is lowered so that the primers can attach to the ssDNA strands. This temperature depends on the melting point of the primers ( $T_m$ ). This step is called annealing. The third step is the extension. The temperature is changed to an optimal temperature for the polymerase enzyme. During this time, the polymerase can bind to the primer and start to synthesise the desired part of the DNA [5]. These three steps in the mentioned order build up a cycle, and a PCR measurement consists of multiple cycles, which can be seen in Figure 1.1.

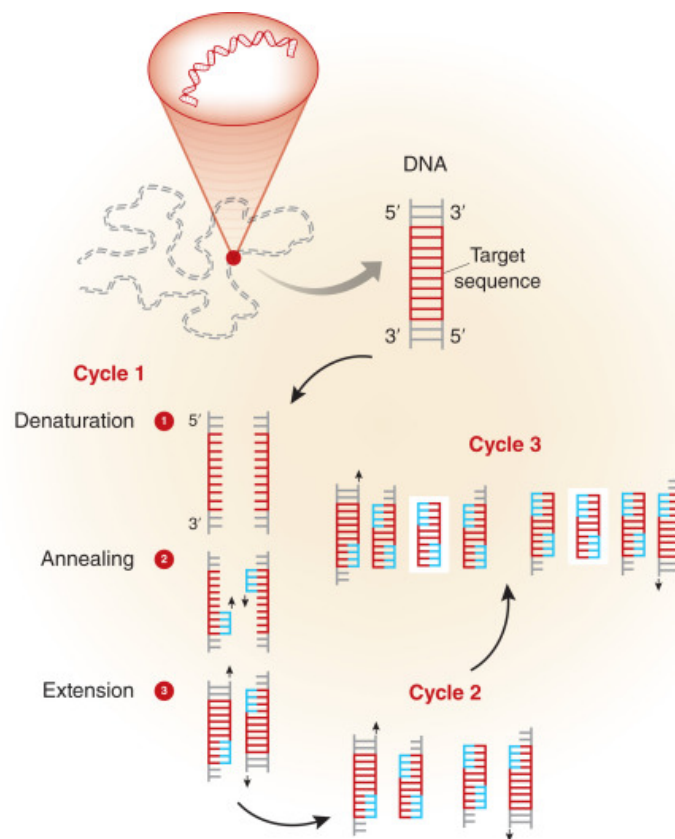


Figure 1.1: Schematic representation of the PCR process flow [20].

## 1.2 PCR on a Chip

The design approaches of modern PCR lab-on-a-chip systems can be separated into distinct categories: well-based PCR chips and continuous-flow PCR chips [7].

Well-based PCR chips work similarly to conventional PCR. The PCR mixture is injected into wells, then the whole chip is heated and cooled repeatedly to the appropriate temperatures, creating cycles [21, 22]. This results in a long thermal-cycling time as the thermal mass remains relatively large.

Continuous-flow PCR chips, on the other hand, move the sample through fixed-temperature zones to achieve the required thermal cycling. This results in a lower thermal mass since only the sample has to be heated. This approach of smaller thermal inertia allows faster thermal cycles and lower energy requirements [7]. These properties are desired in portable  $\mu$ TAS systems, making continuous-flow PCR more convenient.

Continuous-flow PCR chips can be achieved with three different approaches. They can be oscillatory, closed-loop, and fixed-loop devices. The advantage of oscillatory and closed-loop chips is that both are capable of a variable number of thermocycles. This is done by pumping the sample back and forth in chambers of varying temperatures in the first [23], or by moving the sample in a closed loop in the latter [24]. Fixed-loop systems have a nonvariable number of cycles which has to be determined at the point of fabrication. While this is disadvantageous in terms of flexibility, these systems have the potential to achieve much faster thermocycling and are much simpler in design [7]. For these reasons, the design of a continuous-flow fixed-loop PCR chip was chosen for this paper.

### 1.2.1 PCR Inhibition due to Adsorption

PCR inhibition due to adsorption is one of the main hurdles of lab-on-a-chip PCR systems. When PCR components come into contact with the surface of their vessel, they may adsorb to it even in conventional PCR [7, 13–15]. This effect increases as the surface-to-volume ratio increases in the system. Microfluidic devices may have a fraction of the volume of conventional PCR, while also having many times their surface. This makes this problem more prevalent in chip-based PCR solutions. As adsorption lowers the concentration of PCR components, it greatly affects yield and the effectiveness of amplification. If DNA molecules adsorb, it may also cause carryover contamination in subsequent samples [13]. Understanding this phenomenon is essential to PCR chip design in order to minimise the inhibitory effect.

Gonzalez *et al.* [13] extensively studied the interaction of PCR components and the surfaces of polymers. They have confirmed that the inhibitory effect increases with larger surface to volume ratios, and found this relation to be exponential (Figure 1.2). It was also found that lowering the sample volume has the most significant effect on product yield, which is expected, as this greatly increases the surface-to-volume ratio. The findings of Gonzalez *et al.* [13] suggest that the inhibitory phenomenon only affects yield, but not the specificity of the reaction, finding no difference in amplicons of the same PCR mixture, regardless of adsorption interactions.

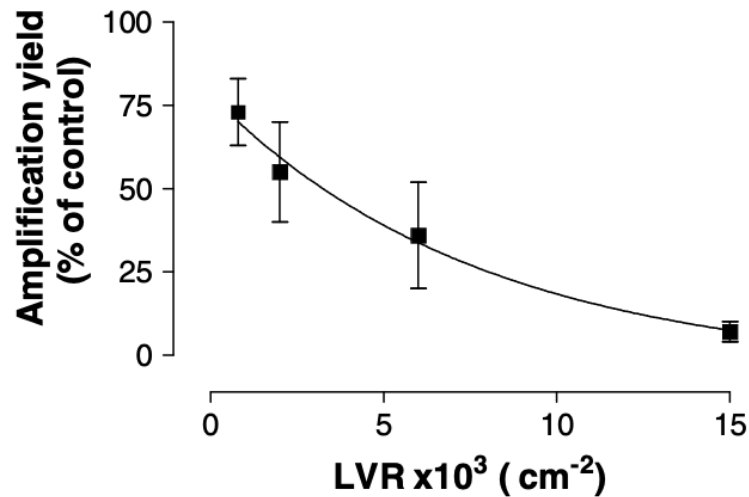


Figure 1.2: Inhibition of PCR yield as a function of length to volume (LV) ratio. PCR samples (20 or 50  $\mu\text{l}$ ) were passed through purified PFA tubing of either 40 cm or 3 m to generate different LV ratios [13]

Gonzalez *et al.* [13] also compared the yields across several different polymers, including fluoroethylene-propylene (FEP), Perfluoralkoxy (PFA), polyetherketone (PEEK), and fluoropolymer (Tefzel). They have found no significant difference between the aforementioned materials. This is possibly due to the materials having close to similar surface chemistries.

It is expected that different materials should interact differently with PCR components. The biocompatibility of commonly used materials in microfluidics is the subject of many papers [13–15]. Kodzius *et al.* [15] assessed how different materials interact with and with which PCR components. The assay included silicon, silicon oxides, glasses, polymers, waxes and adhesives of various kinds. To determine if the template DNA or the DNA polymerase has a bigger impact on inhibition, PCR samples were soaked in the aforementioned materials, with either the template or the polymerase missing, so that they could be added later. Kodzius *et al.* [15] found that the adsorption of DNA polymerase is the main cause of PCR inhibition. Their findings can be seen in Figure 1.3, where inhibition through component adsorption is compared across different materials, by their weighted relative band intensity.

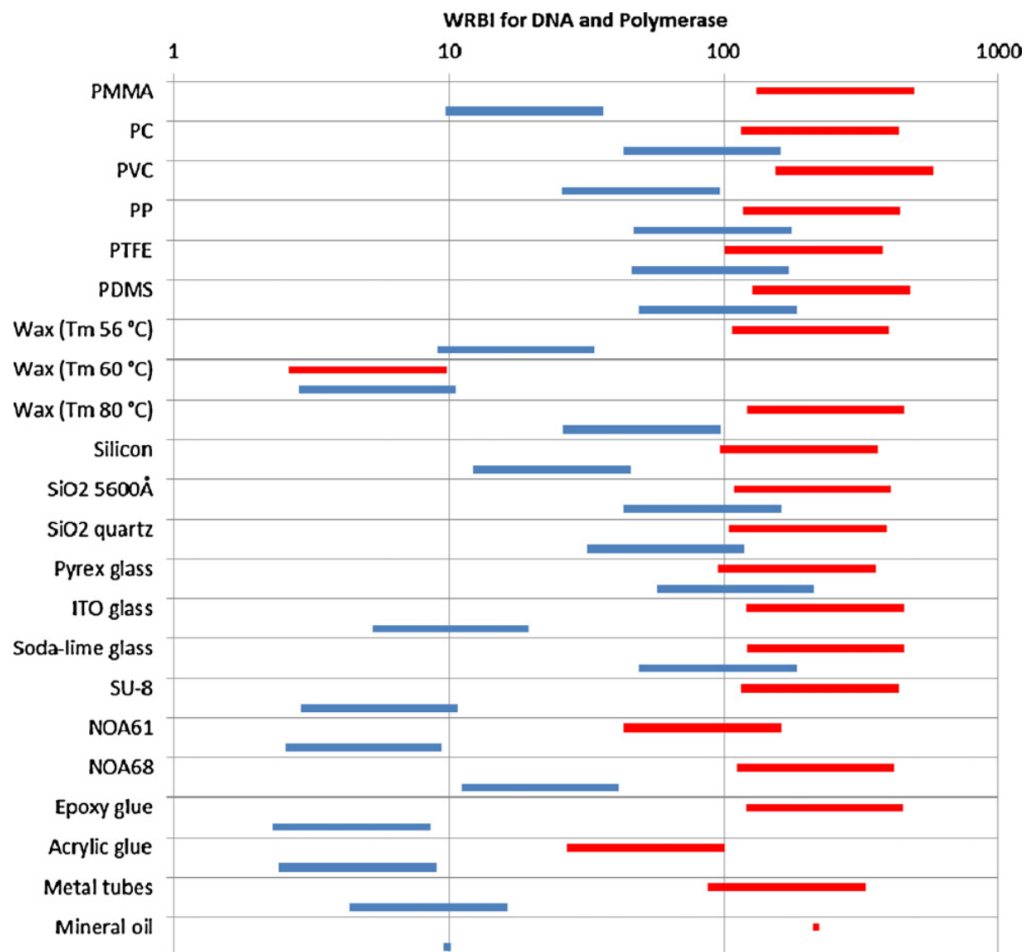


Figure 1.3: PCR inhibition through material interaction with **template DNA** (red bar) and **DNA polymerase** (blue bar). The **DNA polymerase** or **template DNA** was added after the rest of the PCR mixture had been incubated with the material under test. This was to avoid interaction between the material under test and the **DNA polymerase** or **template DNA**. The calculated WRBI (Weighted Relative Band Intensity) range is indicated for each of material. Lower WRBI values indicate inhibition, whereas higher WRBI values mean less inhibition [15].

### 1.2.1.1 Passive and Dynamic Coatings

A common method of preventing adsorption of components is through surface active coatings. Based on the method of applying them, there are two approaches to coatings: passive and dynamic coatings. Passive coatings are applied to the surface of the device either at fabrication or sometime before use. Dynamic coatings, on the other hand, are added directly to one or more of the fluid phases of the microfluidic system, thus dynamically coating the surfaces while in use. Typical coating materials are silanizing agents such as hexamethyldisilazane (HDMS), anti-sticktion agents like Teflon, surfactants, or biological materials like bovine serum albumin (BSA) [17, 25].

A key parameter to consider when choosing coatings for PCR purposes is their biocompatibility. In surfactants, for example, only non-ionic surfactants have been shown not to reduce the extension rate of Taq polymerase [16]. They can be used as a dynamic coating or as a passive one. Added to PDMS before curing has been shown to provide a long-lasting passive solution [26].

BSA is a commonly used component in molecular biology with proven biocompatibility. In PCR, it is used to enhance the specificity of the reaction by reducing the non-specific binding of primers in regions of high CG concentration, and to reduce surface adsorption. Christensen *et al.* [14] have shown that BSA is an effective passive coating on silicon, glass and SU-8, but only for single-use purposes, as its effectiveness falls after the first use (Figure 1.4).

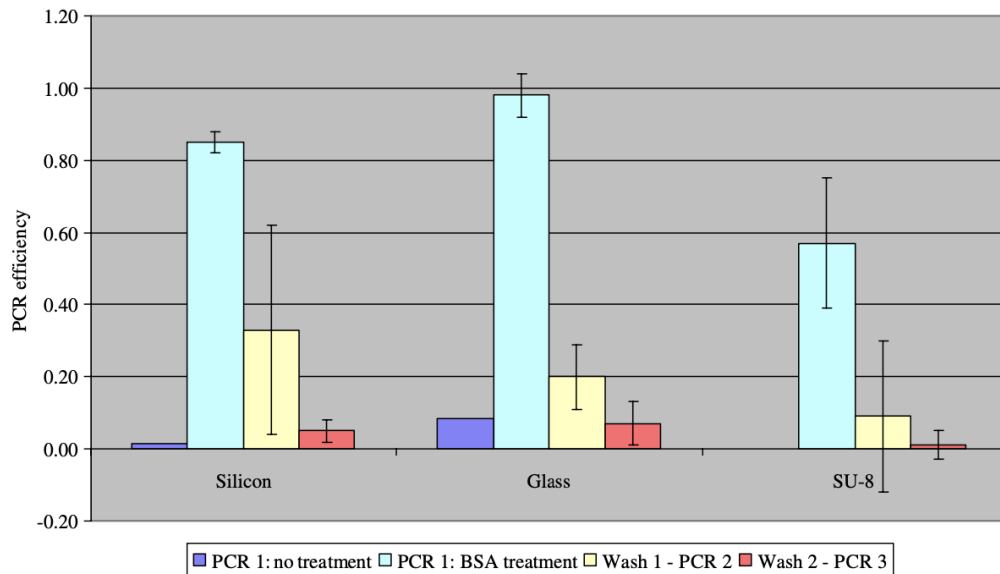


Figure 1.4: The PCR efficiencies after initial BSA treatment and two subsequent washing steps are shown. For comparison, the PCR efficiency with a non-treated sample is also shown. For all three materials, a significant decrease in PCR efficiency is observed after the washing steps indicating that the BSA can be washed off the materials [14].

For prototyping, dynamic coatings are advantageous, as they don't have to be reapplied between runs. Using BSA as a dynamic coating has shown results of varying effectiveness [15, 17]. This is likely due to the fact that BSA is a surface-active molecule, and thus the concentration optimal in reducing inhibition is dependent on the surface-to-volume ratio of the system. Christensen *et al.* [17] have shown that yields close to as of conventional PCR can be achieved using dynamic BSA coatings. They found the optimal concentration to be 10 mg/ml, which is significantly higher than what is typically used in PCR.

### 1.2.1.2 Droplet PCR as adsorption prevention

Another method of preventing inhibition due to PCR component adsorption is droplet PCR [7, 18]. It prevents adsorption by having the aqueous PCR mixture in droplet form in an immiscible phase, such as mineral oil, thus eliminating contact between the components and the channel surface, each droplet acting as an individual reaction vessel [19]. The elimination of short chimeric fragments is also an advantage of droplet PCR. In conventional PCR, homologous regions of gene fragments may recombine, creating short chimeric products. Since microdroplets only contain one or just a few templates, this phenomenon is greatly reduced [19].

### 1.3 Microdroplet Generation

To generate microdroplets, there are many factors to consider: temperature, flow rate, and geometry of the channels. The viscosity and surface tension of the liquid can also influence the generation. [27, 28]

There are two methods of droplet generation considering the external factors: passive and active. In passive generation of droplets, no additional external force is used. We can differentiate the methods by the shape of the channels. There are four geometric shapes: the T-junction, flow-focusing, co-flowing, and step emulsion. The most widely used of these nowadays are T-junctions and flow-focusing structures, which allow for automatic and fast droplet generation. In active generation, an external force is used to break the fluid flow. To create these external forces, a more complex setup is required than that of passive methods. [27]

#### 1.3.1 T-junction

The first passive droplet generation was created by using a T-junction. A continuous oil phase with a perpendicular aqueous phase that forms the T-junction (Figure 1.5). The size and form of the droplets can be manipulated by the geometry of the channel or the flow rate. [27–29]

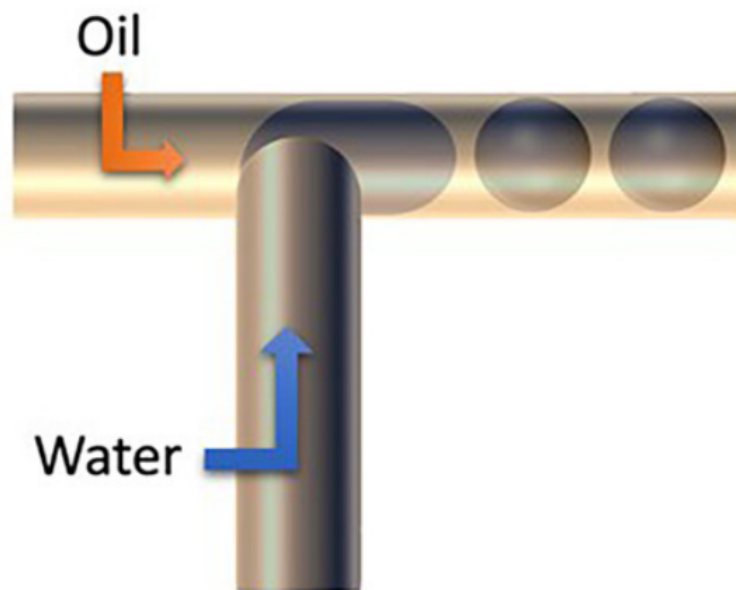


Figure 1.5: Schematic representation of the T-junction structure. [27].

Every droplet is created in the same way in one T-junction with the same parameters. First, the aqueous phase enters the oil phase. Due to pressure and force, a water droplet starts to form in the oil phase. During growth, the droplet starts to take an oval shape, and when the neck of the droplet becomes thin, it breaks off, and without the main aqueous phase, it takes a round shape in the oil and starts to follow the main oil phase stream. After the droplet is released, a new droplet starts to form. This is repeated until the generation parameters change. [28]

Because of the simplicity of creating uniform droplets, the T-junction is widely used in microfluidics currently. The fabrication of the T-junction structure is both uncomplicated and cost-effective. [27, 28]

## 1.4 Lithography

Lithography is a method to fabricate a pattern on a micro- or nanoscale with the use of a physical or digital mask in different materials like oxide, metal, or polymers [30, 31]. In photolithography, the first step is to clean the substrate to eliminate impurities and particles, using methods such as chemical, mechanical, or plasma cleaning. This is crucial to ensure the accuracy and quality of the pattern. After cleaning, the substrate is heated, also known as dehydrating baking, to remove any moisture, which helps the layers adhere properly. The substrate then receives a uniform photoresist coating through spin- or split-coating methods, ensuring even distribution. The coated layer is dried and prebaked to remove any solvents. The photoresist is then exposed to UV light through a photomask, which transfers the pattern from the mask to the substrate. This exposure creates soluble and insoluble areas in a developer, which is then developed using a solution to solidify the pattern. Post-baking further strengthens the adhesion of the photoresist to the substrate, but could also cause deformation, which might be detrimental for smaller structures. The development process may also involve rinsing to remove any residual chemicals, finalising the intricate design. Through this process, photolithography enables the creation of precise and detailed patterns on various substrates [30, 32].

### 1.4.1 UV Lithography

UV lithography is used for transferring patterns onto a substrate using ultraviolet (UV) light. The process has 3 main steps: 1. Coating the substrate with a photosensitive film. 2. Transfer of a pattern to the resist by exposing it with UV light through either a physical shadow mask or a digital version of a shadow mask. 3. Developing the exposed resist to reveal the transferred pattern [32].

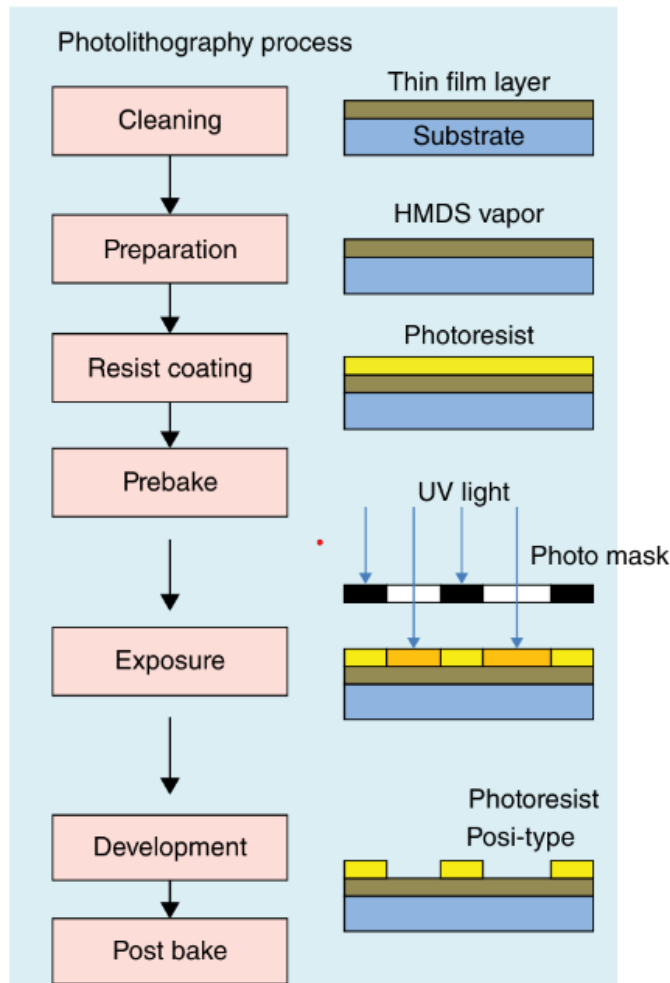


Figure 1.6: Schematic representation of the work-flow of UV photolithography [30].

This process allows the creation of microstructures with pattern sizes ranging from approximately  $1\ \mu\text{m}$  and up, with the specific resolution depending on the resist type, thickness, and complexity of the pattern. The resist, which is a photosensitive material, typically has a thickness between  $0.5\ \mu\text{m}$  and  $200\ \mu\text{m}$ , depending on the application and the desired outcome. The exposure process varies with the equipment used; for mask aligners, the typical exposure time ranges from 10 to 180 seconds per wafer, whereas for maskless aligners, it can take 5 to 60 minutes per wafer. The size of the substrate can vary significantly, with common wafer sizes ranging from small chips as small as  $3\ \text{mm} \times 3\ \text{mm}$  to standard sizes of  $50\ \text{mm}$ ,  $100\ \text{mm}$ ,  $150\ \text{mm}$  and  $200\ \text{mm}$  wafers. However, the resolution is dependent on several factors, including the resist's properties and the thickness of the resist layer, which can significantly influence the final pattern quality.

## 1.5 Dry Etching

Dry Etching is a method of material removal with the use of plasma through chemical and physical etching. As opposed to wet etching, dry etching is capable of anisotropic etching, which is desirable in the fabrication of high aspect ratio structures, such as lab-on-a-chip

devices. Dry etching is commonly used in combination with lithography, where only the areas not protected by the mask are etched.

A common dry etcher is the Reactive Ion Etcher (RIE). It consists of an upper electrode, which is grounded, and a lower electrode, which has a 13.56 MHz AC potential (Figure 1.7). As electrons collide with the neutral molecules of the etching gas, they might get ionised, which releases more electrons in a cascading effect, creating the plasma phase. To the potential, there's a blocking capacitor connected (also known as the platen). This makes electrons collect on the lower electrode, which locally creates a negative potential called the DC potential. This local negative potential repels the electrons, which means there's no plasma close to the lower electrode, but when ions diffuse close enough to it, the potential accelerates them towards the electrode. This directionality is the basis of anisotropic etching [33].

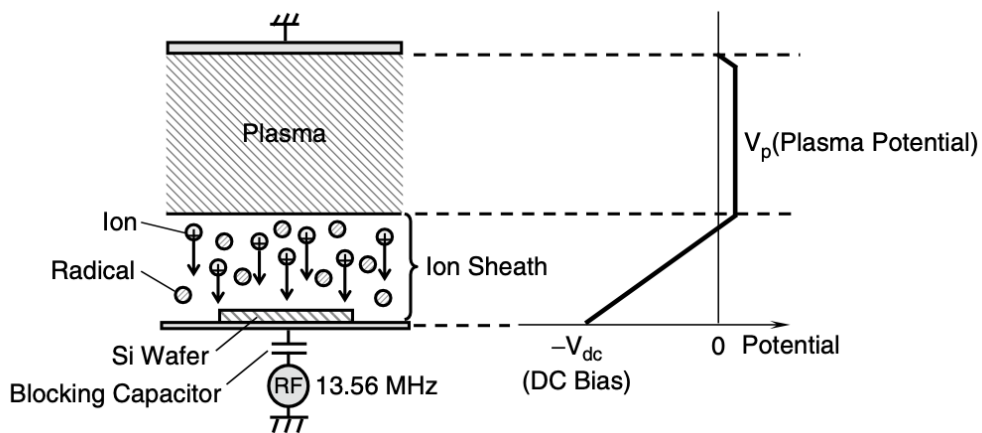


Figure 1.7: Outline of dry etching [33].

Another common dry etch is the Inductively Coupled Plasma (ICP), which works similarly to RIE, but the plasma is created by a coil wound around the reaction chamber. This allows for better control and potentially higher plasma density.

These systems are also coupled with a pump, as lowering the pressure lowers the breakdown voltage of plasma as well, to a point, and on the inlet side are coupled with etching gas sources with mass-flow regulators, so recipes can be selected depending on the etched material and structure (Figure 1.8).

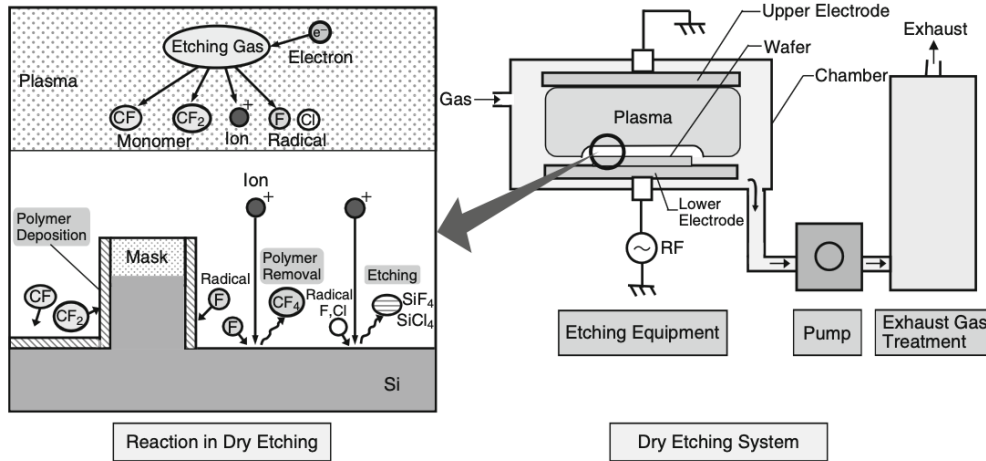


Figure 1.8: Dry etcher layout [33].

To dry etch a material, it has to create a volatile product with the etching gas. When the etching gas reacts with the surface, ions may activate the reaction by breaking bonds or by increasing surface energy. Ions also have a role in helping the volatile product desorb from the surface. Since the ion bombardment is directional due to the DC potential, the etching is directional as well [33].

If the product is not volatile, it may deposit back on the surface, which is referred to a physical sputtering. Another etch reaction is chemical etching, which is caused by neutral molecules or radicals reacting with the substrate in a way that creates a volatile product without the need for ion bombardment. Since these particles are not charged, they collide with the surface due to diffusion, etching the surface isotropically, in all directions [33].

### 1.5.1 Bosch Process

The Bosch Process is a type of Deep Reactive Ion Etching (DRIE), designed to etch deep, high aspect ratio etches. Normally, when etching deep trenches, the depth is limited by the mask being etched away, and the unprotected walls may be etched chemically, breaking the anisotropic profile. The Bosch Process utilises repeating cycles of deposition of passivation, breaking passivation, and etching (Figure 1.9).

In the deposition step, the reaction chamber is filled with  $C_4F_8$ , the radicals of which deposit on the surface of the substrate, creating a protective film. Then, in the break step, the chamber is filled with  $SF_6$ , and the platen power is turned on to create a negative potential, causing ion bombardment, which etches away the passivation film anisotropically, leaving the sidewalls protected. Finally, in the etching step,  $F$  radicals chemically etch the unprotected surfaces, deepening the trench [33].

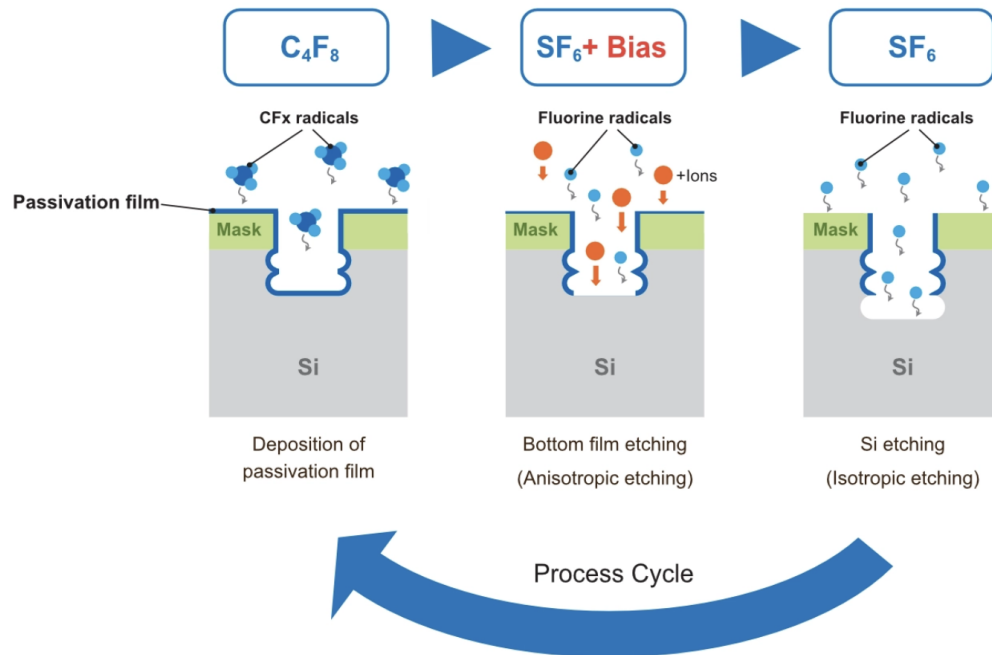


Figure 1.9: The Principles of the Bosch Process [34].

Due to the isotropic nature of the etch step, the Bosch process creates a "scaloped" wall profile, but it is capable of creating extremely high aspect ratio anisotropic structures.

# Chip Design 2

## 2.1 PCR chip structure

The design of a continuous-flow fixed-loop droplet-based PCR chip was selected for this paper. The device consists of a single channel meandering through three well-defined temperature zones, corresponding to the temperature ranges used in conventional PCR. These zones are arranged in band-like regions, starting with the denaturation, followed by the extension, and finally the annealing region. The desired temperature gradient is created using two heating elements and three strategically placed copper plates to achieve near-constant temperature regions across large areas.

As the denaturation and annealing processes are near instantaneous, the time spent in the corresponding regions can be minimised to accommodate more time spent in the extension region. This is achieved by having additional meanders in the extension region, effectively increasing the length of the channel in that zone. This addition allows for higher flow rates, making the whole process faster. The above concept is demonstrated in Figure 2.1.

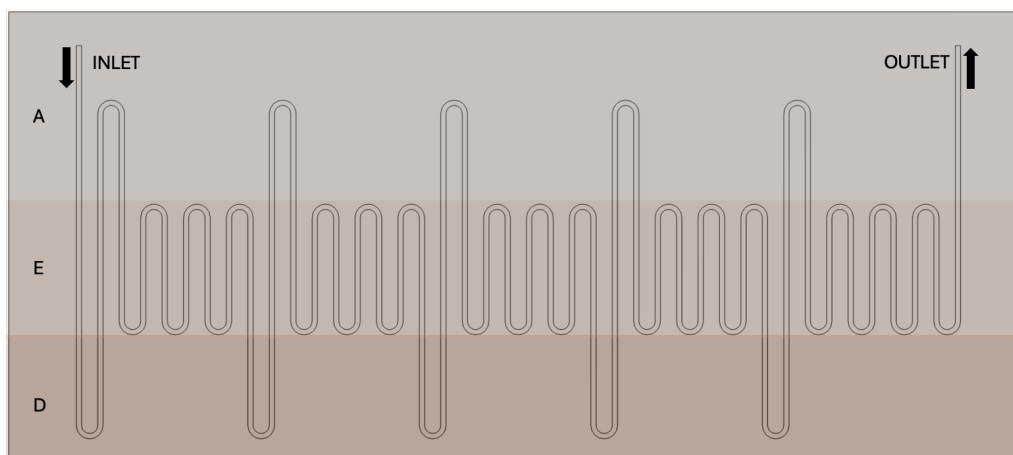


Figure 2.1: PCR chip schematic diagram. sample inlet, sample outlet, denaturation temperature zone (D), extension temperature zone (E), annealing temperature zone (A).

The theoretical workings of the chip are the following: The sample enters the chip in the annealing zone and passes directly to the denaturation zone, where the double-stranded DNA denatures and splits into single-stranded DNA templates. Primers then attach to these templates in the following annealing zone. The sample then passes through the meandering extension zone, where the primers are extended, completing a single PCR cycle. The cycles are repeated to achieve the desired number of cycles. The amplified sample exits the chip from the final extension zone through the annealing zone, avoiding

denaturation to keep the product intact.

A PCR chip was designed using the above concept. The chip's dimensions are 75 mm by 33 mm, and it is capable of 25 PCR cycles. The addition of an integrated T-junction droplet generator was made to enable droplet-based PCR as well. The main channel is 150  $\mu\text{m}$  by 150  $\mu\text{m}$ , while the T-junction at the inlet is 75  $\mu\text{m}$  wide and 150  $\mu\text{m}$  deep. The channels are evenly spaced, and the channel meanders seven times in each extension zone to maximize the sample's time spent in them. The total channel volume is 19.01  $\mu\text{l}$ . The layout of the designed chip can be seen in Figure 2.2.

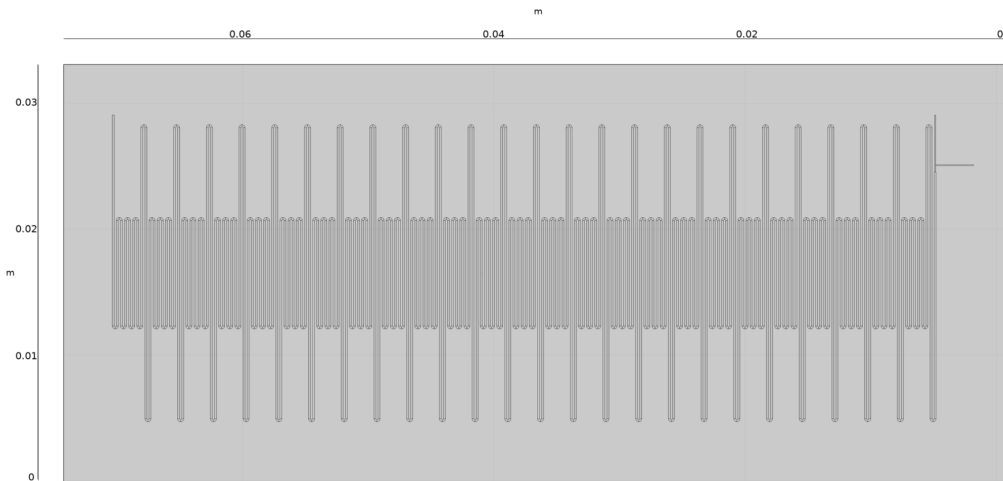


Figure 2.2: COMSOL model of the PCR chip's channel layout. The chip's inlet is on the right side, while the outlet can be seen on the left.

The chip consists of two parts, as seen in Figure 2.3, a chip base that has the channel etched into it, and a Polydimethylsiloxane (PDMS) coverplate. The material of the base is not predetermined, as it is dependent on the chosen fabrication method (PMMA, silica, and PDMS were considered).

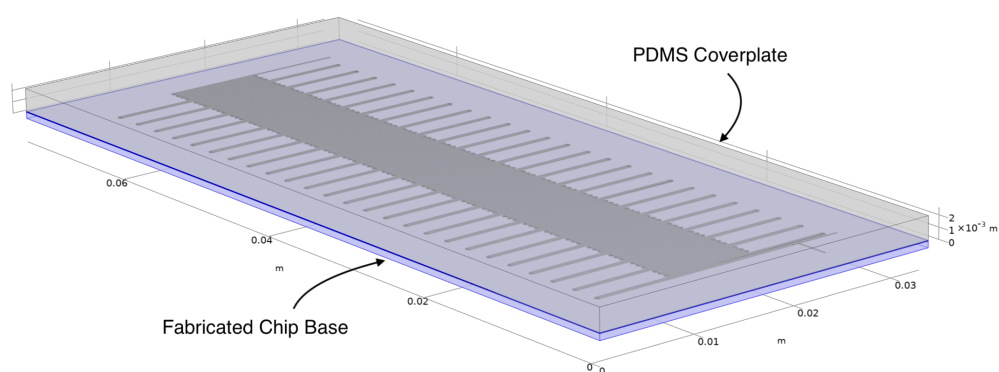


Figure 2.3: COMSOL model of the PCR chip's 3D structure. The chip has 2 layers: chip base (bottom, material to be determined by fabrication method), PDMS (top).

## 2.2 Supporting Components

The chip requires several additional components to function properly. Independent injection and heating systems were designed for easier prototyping, which can then be switched in and out of the 3D printed holder case.

### 2.2.1 Chip Holder

Correct positioning is key to the function of the device. The extension region is established by two heating elements placed 17 mm from each other, and three copper blocks. To achieve this, a 3D-printed chip holder was designed as shown in Figure 2.4.

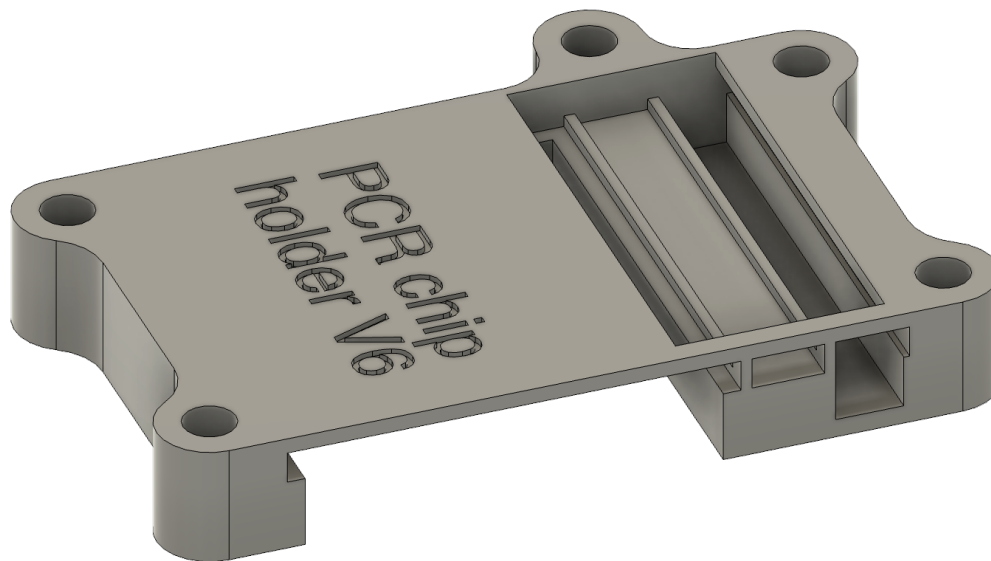


Figure 2.4: Model of 3D-printed chip holder, designed to correctly position the device's components.

The components are slotted into the holder and then pressed together using a laser-cut PMMA cover plate fastened with five M8 bolts.

### 2.2.2 Heating Elements

The discrete temperature zones of the device are created by three copper plates and two heating elements. Since the PCR chip is only 33 mm wide and the desired temperature difference between its two edges is around 50 °C, overheating could prove problematic. To combat this, we used one resistive heating element and one Peltier cell. The Peltier cell effectively only cools the device to annealing temperatures, not heats it.

For stable and predictable heating, proper thermal contact is essential. For this, a combination of thermal pastes and thermal clays is used, while the PCR chip is pressed onto the copper plates by the cover plate of the holder.

### 2.2.3 Injection System

To control the flow of the two injected phases in the PCR chip, three syringe pumps are used. One is connected directly to the inlet of the continuous phase, while another is connected to the inlet of the dispersed phase through an analytical injection valve with a 25  $\mu\text{l}$  injection loop to reduce dead volume as much as possible. The third is connected to the outlet to create a negative pressure, reducing stress across the chip, and to act as a sample collector. The inlet syringes are filled with mineral oil to propel the sample through the device. A schematic diagram in Figure 2.5 illustrates the injection system used in this paper.

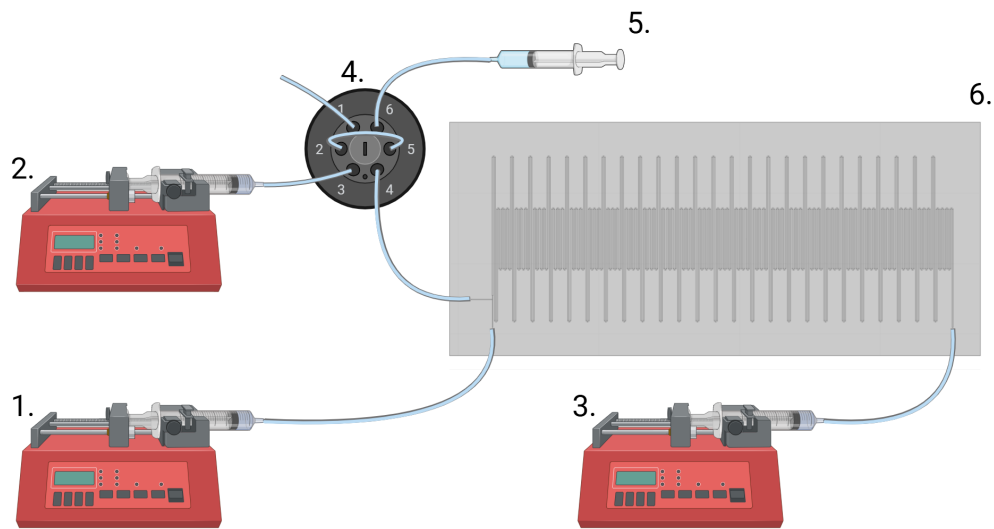


Figure 2.5: Schematic diagram demonstrating connections of the injection system. Syringe pump (1-3.), analytical injection valve (4.), PCR mixture (5.), PCR chip (6.). PCR mixture inlet (4.6), PCR mixture injection loop (4.2-4.5), mineral oil inlet (4.3), valve outlet (4.4), waste outlet (4.1).

#### 2.2.3.1 Flow velocity

The extension rate of a DNA polymerase ( $r_{ext}$ ) is a parameter representing the number of nucleotides the primer is extended by each second. Considering this, one can calculate the theoretical flow velocity ( $v$ ) required for a given fragment length. As droplet formation is dependent on the ratio of the flow velocity of the continuous and dispersed phase, but not the total flow velocity [35], the theoretical flow velocity ( $v$ ) refers to the total flow velocity.

The extension rate of Taq polymerase is greatly influenced by many factors, such as temperature, pH, loss of polymerase due to adsorption, presence of monovalent cations,  $T_m$  depressors, DNA dyes and magnesium ion concentration [16]. Although most of these parameters are easily controlled, the loss of polymerase due to adsorption could prove problematic. Due to this, the extension rate of Taq polymerase is assumed to be between 60 and 150 nucleotides a second. This can be used to set initial flow velocities that later can be optimised experimentally.

To calculate the theoretical flow velocity, only the volume and the required time spent in each extension subcycle are needed. The volume ( $V_{ext}$ ) is 0.4604  $\mu\text{l}$ . The time needed in

the subcycle is the fragment length ( $l$ ) divided by the extension rate. This gives us the following formula:

$$\nu = \frac{V_{ext} \cdot r_{ext}}{l} \quad (2.1)$$

Using  $r_{ext}=60, 150$  nt/s and  $l=907$  nt, the calculated theoretical flow velocity is 1.83 to 4.57  $\mu\text{l}/\text{min}$ , which gives an expected retention time of 4.16 to 10.39 minutes.

# Methods & Materials 3

Table 3.1: Chemicals and items used in this project.

Chemical	Cas no.	Lot no.	Supplier
Tryptone	91079-40-2	N0091W	VWR
Yeast extract	8013-01-2	M0186W	VWR
Sodium chloride	7647-14-5	17L184138	VWR
Agar	9002-18-0	Lot no.	Sigma-Aldrich
Ampicillin	69-53-4		In-house stock
Tris base	77-86-1		Sigma-Aldrich
Acetic acid	64-19-7		In-house stock
EDTA pH8	6381-92-6		In-house stock
Agarose	9012-36-6	19G0256361	VWR
Ethidium Bromide	1239-45-8	SLBF7132V	Sigma-Aldrich
6x Loading dye	B7024S (Catalog no.)	0411606	New England BioLabs
Generuler <sup>TM</sup> 1 kb DNA Ladder		00032587	Fermentas
Sodium Acetate	127-09-3		In-house stock
Paraffin oil	8012-95-1	STBG7873	Sigma-Aldrich
Fluorescein Sodium Salt	518-47-8	SHBN9209	Sigma-Aldrich height

Table 3.2: Chemicals used for PCR.

Chemical	Cas no.	Lot no.	Supplier
dNTPs mix			New England Biolabs
<i>MgCl</i> <sub>2</sub> (50mM)	7786-30-3	00811840	Thermo Fisher Scientific
10x PCR buffer		00933107	Thermo scientific
10x CutSmart buffer	10043914		New England Biolabs
AccuGene®Molecular biology water	7732-18-5	8MB248	Lonza
GeneJET plasmid miniprep kit		00714520	Thermo Fisher Scientific.

Table 3.3: Enzymes, plasmids, and cells used in this project.

Biological chemical	Description	Supplier
<i>Taq</i> polymerase	9012-90-2	Thermo Fisher Scientific
<i>Escherichia coli</i> DH5 $\alpha$	fhuA <sub>2</sub> $\Delta$ (argF – lacZ) U <sub>169</sub> phoAglN <sub>44</sub> $\psi$ <sub>90</sub> $\Delta$ (lacZ)M15 gyrA96 recA1 relA1 endA1 thi-1 hsdR17	New England Biolabs

Table 3.4: Primers used for PCR. Supplied by TAG Copenhagen A/S.

Name	Sequence	$T_m$ °C
pET11a2 for	5'-GAT GTC GGC GAT ATA GGC-3'	50.3
pET11a1 rev	5'-CCT CCT GCG GGA TAT CCG-3'	52.6

### 3.1 Fabrication Using Laser Ablation

Initially, fabrication using laser ablation was considered, as this method does not require a clean laboratory, which at the time we had no access to.

An EduARTx1250 90 W CO<sub>2</sub> was selected for the task. To fabricate the chip base, our design needed to be etched into a 5 mm polymethyl methacrylate (PMMA) sheet. As the equipment was never used in similar applications, we first had to assess its eligibility for our purposes. To do so, several tests were carried out to determine the characteristics of the laser cutter and the correlations of laser power and etch speed to the depth and width of the etch lines. A meandering pattern with progressively smaller turn radii was developed for the tests, so the distances between the lines were 5, 1, 0.5, 0.1 and 0.05 mm. The tested power, speed and pass number combinations can be seen in Table 3.5.

Table 3.5: Experimental parameters tested on EduARTx1250 laser cutter. Sample no: Sample number, Power min (%): minimum laser power during sharp turns, percentage of 90 W, Power max (%): maximum laser power in straight lines, percentage of 90 W, Speed (mm/s): speed the laser head is moved at, Passes (n): number of passes over the sample.

Sample no.	Power min. (%)	Power max. (%)	Speed (mm/s)	Passes (n)
1.	9	9	10	5
2.	10	10	60	1
3.	10	10	40	1
4.	10	10	10	1
5.	11	11	10	1
6.	12	12	10	2
7.	13	13	10	2
8.	15	15	150	1
9.	15	15	100	1
10.	10	15	80	1
11.	15	15	10	1
12.	18	18	60	1
13.	20	20	100	1
14.	20	20	80	1

### 3.2 Fabrication Using UV Lithography and Dry Etching

In addition to laser ablation, a combination of ultraviolet lithography and dry etching was also considered to fabricate the chip. This alternate approach was carried out at the Technical University of Denmark's (DTU) Nanolab facility.

For the process, four 4" silicon wafers with a thickness of  $525 \pm 25 \mu\text{m}$  were selected. Two approaches to fabricating the final product were considered. One is to use the etched wafers as reusable moulds to create PDMS chips using them, and the other is to use the etched wafers as chips directly. To achieve this, two wafers were etched with the negative of our design, while the other two were etched with the positive of it.

### 3.2.1 UV Lithography

As a spin coater, a Gamma 2M cluster from Süss MicroTec was used with spin coating, HDMS vapour deposition, and baking modules. HDMS was then deposited on the wafers, which were then coated with 4  $\mu\text{m}$  of nLOF 2020 negative resist. To achieve this thickness, 852 rpm for a duration of 30 seconds was used. After this, the wafers were soft-baked at 110 °C for 60 seconds.

The wafers were then exposed using the MLA150 WMII maskless aligner. The machine's process parameters were set to optical autofocus, fast exposure mode with an exposure dose of 450 mJ/cm<sup>2</sup>. No defocus was used.

A post-exposure bake at 100 °C for 60 seconds was performed prior to development, after which the wafers were developed with AZ 726 MIF (2,38 % Tetramethylammonium hydroxide in water) for 60 seconds, using the single puddle method.

### 3.2.2 Dry Etch

The dry etching process was carried out on SPTS Technologies Ltd. Pegasus deep reactive-ion etching (DRIE) system using the Bosch process, allowing for high aspect ratio etching. To achieve the desired dimensions, DTU Nanolab's ProcessA [36] recipe was followed, which uses the parameters listed in Table 3.6.

Table 3.6: Parameter list of ProcessA for DRIE-Pegasus. Parenthesis: held for specified time, arrows: ramping from one value to another.

Parameters	Step 1.		Step 2.	
	Etch	Deposition	Etch	Deposition
Gas flow (sccm)	$SF_6$ 350 (1.5 s) 550	$C_4F_8$ 200	$SF_6$ 350 (1.5 s) 550	$C_4F_8$ 200
Cycle time (s)	7	4	7	4
Pressure (mtorr)	25 (1.5 s) 90 $\rightarrow$ 150	25	25 (1.5 s) 150	25
Coil power (W)	2800	2000	2800	2000
Platen power (W)	120 $\rightarrow$ 140 (1.5) 45	0	140 (1.5) 45	0
Cycles	11 (fixed)		variable	
Temperature (°C)	20		20	

Since the etch rate is dependent on the etch load, one mould and one chip wafer were used to measure the etch rates specific to them. For this, 44 cycles were selected. Following that, the mould wafers were etched with 93, and the chip wafers were etched with 30 cycles to achieve the desired depth of 150  $\mu\text{m}$ .

### 3.2.3 Post Processing

For easier release, the mould wafers were coated with Perfluorodecyltrichlorosilane (FDTS) using molecular vapour deposition (MVD). This was carried out with the Applied Microstructures MVD 100 system.

PDMS chips, using the mould wafers, and PDMS cover plates were created, which were then bonded using plasma bonding to either a glass surface in the case of the moulded

chips, or to the etched chips in the case of the cover plates.

### 3.3 Fabrication of Supporting Components

#### 3.3.1 Chip Holder

A chip holder body was 3D printed for the purpose of keeping the chip and the heating elements in their proper position and to provide better thermal contact between them. To achieve this, we used an ELEGOO Staurn 3 Ultra resin printer with 3DE Premium Standard Clear resin. Additionally, a cover plate was laser cut from a 5mm polymethyl methacrylate (PMMA) sheet, which can be fastened to the holder using five M8 bolts.

#### 3.3.2 Temperature Control System

In order to achieve the desired temperature gradient across the chip, the following temperature control system was created. On the melting side of the chip, a 6,8 ohm resistor was used, regulated by a Carel ir33 controller. On the annealing side, a 78,7 W, 8 A, 15,7 V Peltier module was used to cool the chip to annealing temperatures. The Peltier module was cooled by both a passive radiator and a PC fan, and was regulated by a TLK33 Peltier cell controller by Ascon Tecnologic. Two RS PRO PT100 RTD platinum sensors were used to monitor the temperatures of the two heating elements. The sensors were attached to the heating elements with thermal clay.

Three 5 mm thick copper plates were cut to achieve the step-like temperature gradient profile on the chip. The plates were then attached to the heating elements using thermal paste, after which thermal clay was added to their top side for better thermal contact between the components and the chip.

#### 3.3.3 Injection System

To precisely propel samples through our device, three New Era SyringeONE:100 High Pressure Programmable Syringe Pumps were selected. One of these was directly connected to the chip using 1/16" PTFE microfluidic tubing, while another was connected through a CHEMINERT C22Z-3186 6-port analytical valve to allow sample injection. The third one was connected to the outlet of the device to create a negative pressure and to collect the product. The sample loop was cut to 25  $\mu$ l in volume. Both inlet syringe pumps were fitted with 1 ml syringes filled with paraffin oil to propel the low-volume aqueous sample through the PCR chip, while the outlet was fitted with an empty syringe. The analytical valve was connected to the dispersed phase inlet of the PCR chip's T-junction, while the other was connected to the continuous phase inlet.

The complete experimental setup can be seen in Figure 3.1.

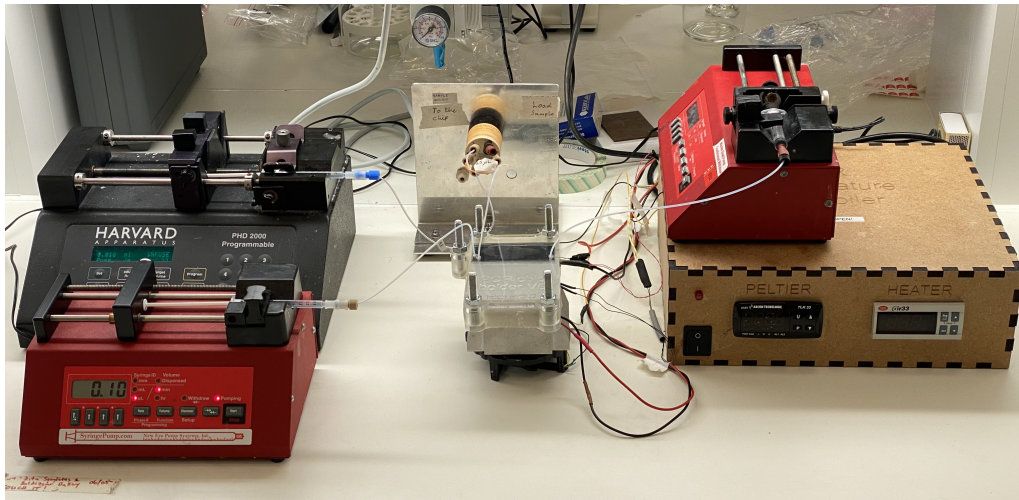


Figure 3.1: Picture of the experimental setup.

### 3.4 Polymerase Chain Reaction

During the PCR experiment, a 50  $\mu\text{l}$  PCR mixture was prepared (Table 3.7). To reduce the adsorption of the PCR mixture in the microfluidic PCR chip, Human Serum Albumin (HSA) was added to the PCR mixture in a concentration of 10 mg/ml. Due to the unavailability of BSA, HSA was used instead. To stabilise the droplets, 1% Triton X-100 was added to the paraffin oil used. The general PCR followed the steps as can be seen in Table 3.8. During the PCR, a pFCPEX1D plasmid DNA template was used with primers (Primer 1 as pET11a1 rev and Primer 2 as pET11a2 for).

Table 3.7: PCR mixture.

Component name	Stock concentration	Volume ( $\mu\text{l}$ )	Volume ( $\mu\text{l}$ )
dNTP	20 nmol/ $\mu\text{l}$	2	4
$MgCl_2$	25mM	6	12
10x PCR buffer		5	10
Template		1	1
Primer 1	100 $\mu\text{M}$	0.5	1
Primer 2	100 $\mu\text{M}$	0.5	1
Taq polymerase		0.5	0.5
Molecular biology water		34.5	70.5
Total volume		50 $\mu\text{l}$	100 $\mu\text{l}$

Table 3.8: One PCR cycle. Steps 2 - 4 are repeated 25 times to complete a PCR process.

Order	Temperature ( $^{\circ}\text{C}$ )	Time
1.	94	5 min
2.	94	30 s
3.	48	30 s
4.	72	1 min
5.	72	7 min
6.	4	Until removed

To see the product of the PCR experiment, we used gel electrophoresis. The gel was made from a 1% Agarose solution with 0.5  $\mu\text{l}$  Ethidium bromide. A 1 kb DNA ladder and a 100

bd DNA ladder from New England BioLab were used as a size marker. The samples were prepared as 5  $\mu$ l PCR product mixed with 1  $\mu$ l of Purple Loading Dye from Nem England BioLab and run at 95 V for approximately 40 minutes.

## 4.1 Laser Ablation Approach

Tests to determine the efficacy of fabrication using the EduArtx550 laser cutter were conducted using a meandering pattern with progressively smaller turn radii.

Of the fourteen experiments conducted, only six were potential candidates for further investigation. Using the parameters of 20% power and 100 mm/s writing speed resulted in channels appearing wider than desired, with a large amount of debris on the surrounding surface, and a great discrepancy in the width of turns compared to straights. Lower powers produced less debris and narrower channels, while lower speeds reduced the width deviation across the channel, as seen in Figure 4.1.

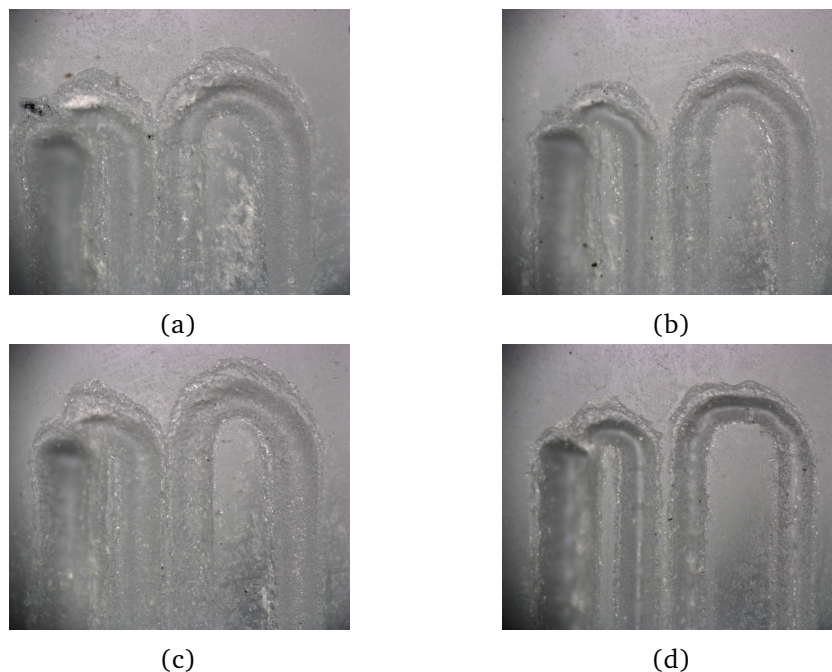


Figure 4.1: Channels etched into PMMA using different parameter combinations on the EduARTx1250 90 W laser cutter. a) power: 20%, speed: 100 mm/s; b) power: 20%, speed: 80 mm/s; c) power: 18%, speed: 60 mm/s; d) power: 15%, speed: 10 mm/s.

As the channels got narrower, the irregularity of their shape became more apparent. To combat this, lower powers with multiple passes were used. As seen in Figure 4.2, etching with power settings lower than 13% is not viable as the 12% channel is very shallow and wide, while the 11% test barely shows any structural change. We can also see that two

passes do not improve the channel's shape, and channels always overlap below 0.5 mm turn diameters. These seem to be limitations of the instrument.

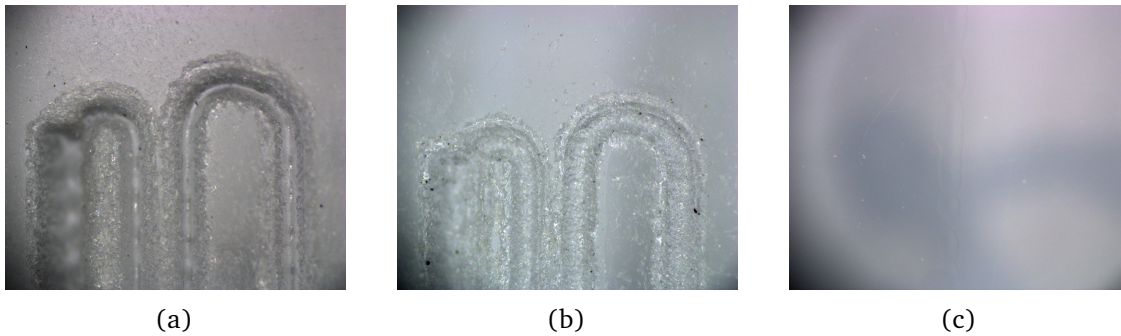


Figure 4.2: Channels etched into PMMA using different parameter combinations and two passes on the EduARTx1250 90 W laser cutter. a) power: 13%, speed: 10 mm/s; b) power: 12%, speed: 10 mm/s; c) power: 11%, speed: 10 mm/s.

Ultimately, the laser ablation approach was deemed unviable due to the lack of resolution and unreliability.

## 4.2 Heat Distribution Simulations

Simulations of heat distribution were conducted in COMSOL 6.3 [37], using Heat Transfer in Liquids and Solids and Laminar Flow Physics modules. Since our designed holder is a material with low thermal conductivity, it was not included in our model. Radiation was also neglected because the holder acts as a barrier between the copper blocks.

The model contains two 1x1x75 mm ceramic heating elements to simulate the Peltier and resistive heaters. These were defined as isothermal domains set to 48 and 94 °C, respectively. The thermal contact with the copper blocks was simulated with constant temperature boundaries, meaning the function of the heater blocks is visualisation only. To establish the distinct temperature regions, three 12x2x75 mm copper blocks were placed 25 mm gaps inbetween them. Finally, the exact geometric model of our silicon chips was placed on top. The layout of the simulation can be seen in Figure 4.3.

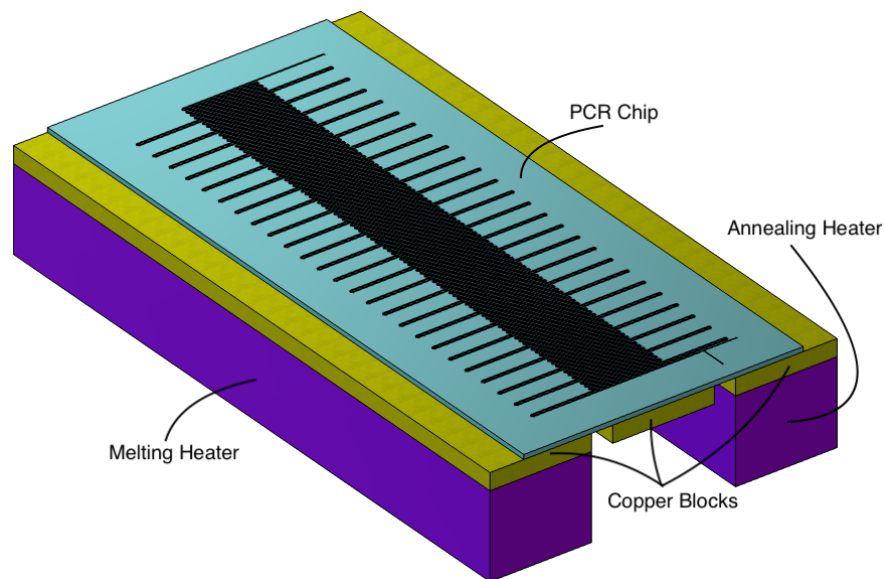


Figure 4.3: Visualisation of simulated COMSOL model. Consisting of: melting heater (purple, left), annealing heater (purple, right), copper blocks (yellow), PCR chip (cyan)

To determine the necessity of the copper blocks in establishing the temperature regions, a simulation was carried out without them. Figure 4.4, the heat map of the aforementioned simulation, shows a continuous temperature gradient across the chip.

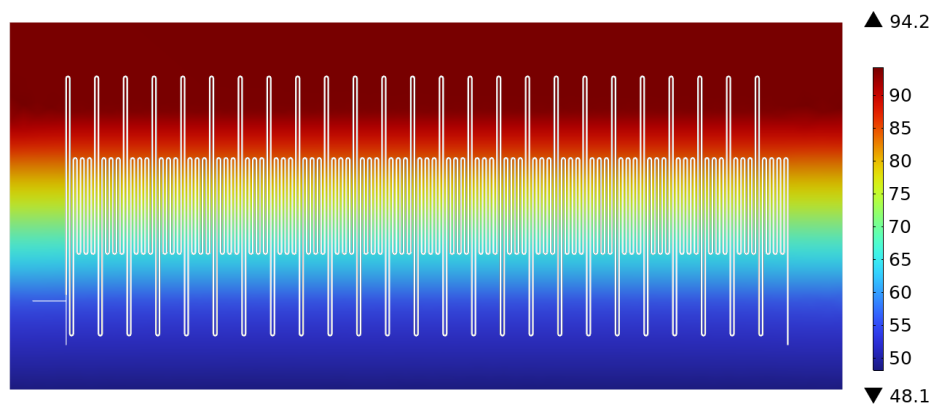


Figure 4.4: Temperature map of the chip (°C) with no copper blocks used.

The temperature profile of a single PCR cycle can be seen in Figure 4.5. A "single PCR cycle" is defined as one period of the chip's channels, starting at a denaturation section (path length = 0 to 0.03 m), continuing through an annealing section (path length = 0.03 to 0.05 m), and finally ending in an extension section (path length = 0.05 to 0.1 m). In the figure, a high temperature variance can be observed from 65 to 85 °C. As temperatures as high as 85 °C can cause a significant portion of the dsDNA to melt [38], while 65 °C is too high for primers to anneal, the use of copper blocks was judged to be essential.

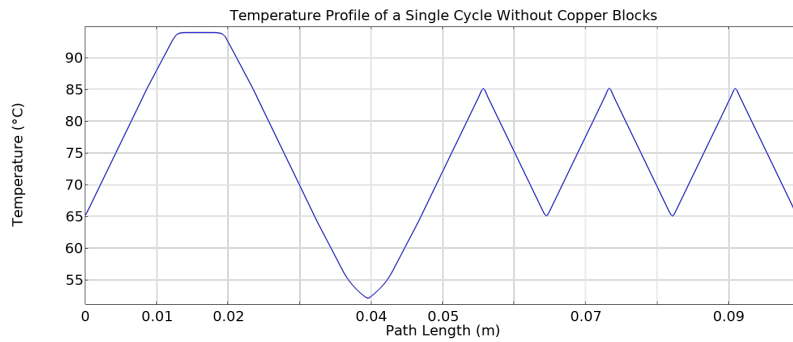


Figure 4.5: Temperature profile of a single PCR cycle without the use of copper blocks. Temperature ( $^{\circ}\text{C}$ ) in terms of distance travelled in the channel (path length (m)). Melting zone (path length = 0 to 0.03 m), annealing zone (path length = 0.03 to 0.05 m), extension zone (path length = 0.05 to 0.1 m)

The same model with the use of copper blocks was then investigated. Distinct temperature regions were established as shown in Figure 4.6.

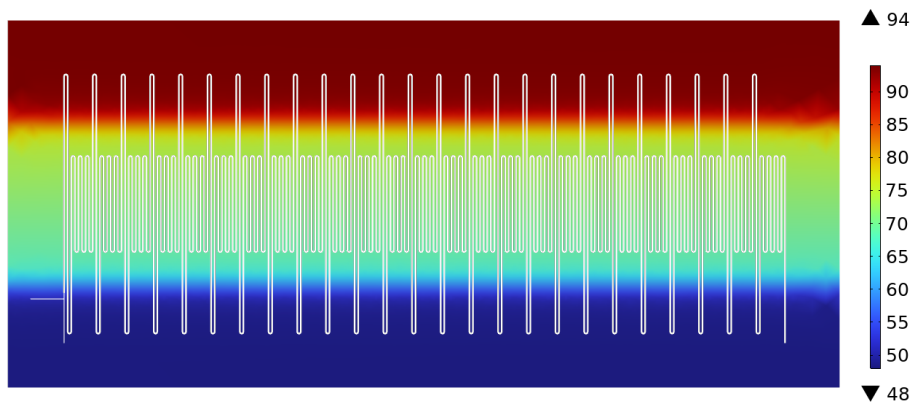


Figure 4.6: Temperature map of the chip ( $^{\circ}\text{C}$ ) with copper blocks. Melting zone (red), extension zone (green), annealing zone (blue)

On the temperature profile plot (Figure 4.7, it can be observed that the temperature regions are much better separated as shown by the narrow melting peaks and annealing valleys. This greatly reduces the "dead volume", where the temperature is of undesired values, which allows the sample to spend more time in the three temperature zones, especially the extension zone, making higher flow velocities possible. The temperature variance of the extension region is also improved, now ranging from 70 to 73,5  $^{\circ}\text{C}$ , eliminating significant dsDNA melting in the section.

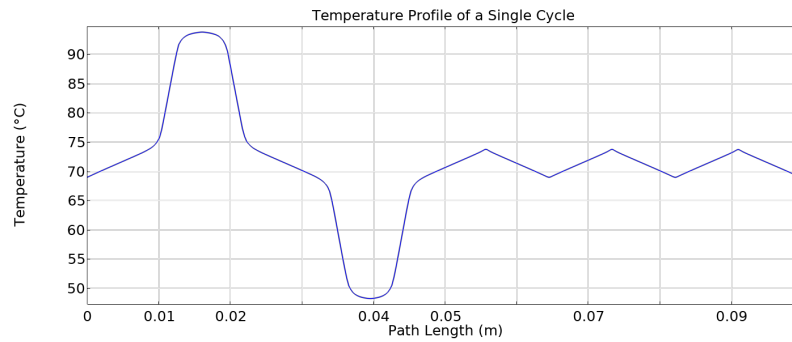


Figure 4.7: Temperature profile of a single PCR cycle with the use of copper blocks. Temperature ( $^{\circ}\text{C}$ ) in terms of distance travelled in the channel (path length (m)). Melting zone (path length = 0 to 0.03 m), annealing zone (path length = 0.03 to 0.05 m), extension zone (path length = 0.05 to 0.1 m)

The time required to reach equilibrium temperatures was also taken into consideration. All of the simulations were carried out after 1800 seconds to allow the system to reach its equilibrium. In Figure 4.8, it can be observed that if the heating elements have reached their respective temperatures, the rest of the chip, starting at  $20^{\circ}\text{C}$ , requires only about 15 seconds to establish the extension zone and reach equilibrium. This means that even if the room temperature chip is placed on the hot heating elements, only a few seconds of preheating is required. In practice, accounting for imperfect thermal contacts, it is still expected that the chip closely follows the temperature of the heaters.

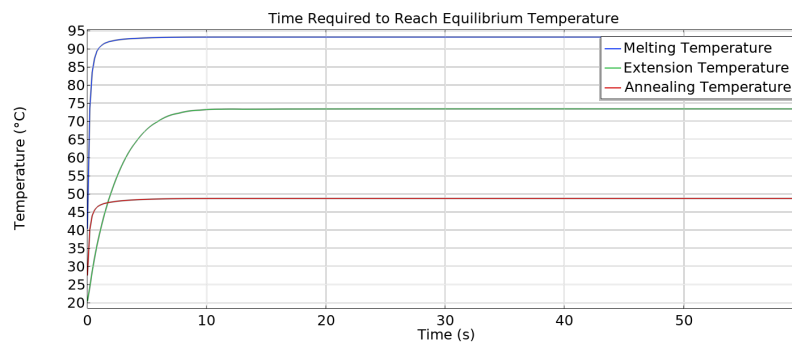


Figure 4.8: The time (s) required to reach equilibrium temperature ( $^{\circ}\text{C}$ ) in each region. Melting zone (blue), Extension zone (green), Annealing zone (red).

The function of the central copper block is to establish the extension zone. Its position between the melting and the annealing heaters determines its average temperature. Figure 4.9 demonstrates the relation between moving the copper block either towards the melting or the annealing side of the chip, and its temperature.

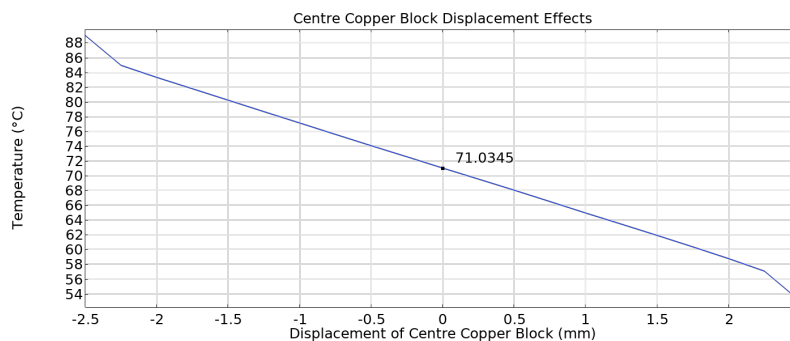


Figure 4.9: The effects of displacing (mm) the central copper block on the average temperature (°C) of the extension zone.

A linear relation can be observed between the temperature of the extension region and its position among the heaters. As different primers might require different annealing temperatures, and different DNA polymerases require different extension temperatures, the ability to establish any temperature profiles is essential. Moving the central copper block allows us to select any temperature for the three zones within reason.

### 4.3 Morphology of the Fabricated Chips

Four wafers, each containing 2 chips, were fabricated at DTU Nanolab. Both the negative and the positive of our design were used to create moulds for the purposes of casting PDMS chips, and to fabricate chips where the channels are etched into silicon.

As the etch rate is dependent on the etch load [33], and one mould and one chip wafer were used to measure the specific etch rate for the designs. With 44 cycles of etching, the mould was  $81 \mu\text{m}$ , and the chip was  $198 \mu\text{m}$  deep. After adjusting for the target  $150 \mu\text{m}$ , 93 and 30 cycles were used to fabricate moulds  $151 \mu\text{m}$  deep and chips  $148 \mu\text{m}$  deep.

Microscope pictures of the etched chips are collected in Figure 4.10 and 4.11.

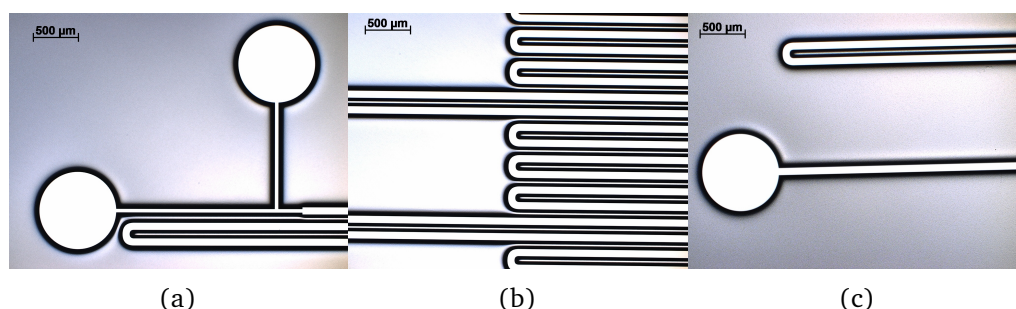


Figure 4.10: Microscope pictures of a mould wafer in 2.5X magnification. T-junction and inlets (a), channels of the extension region (b), outlet (c).

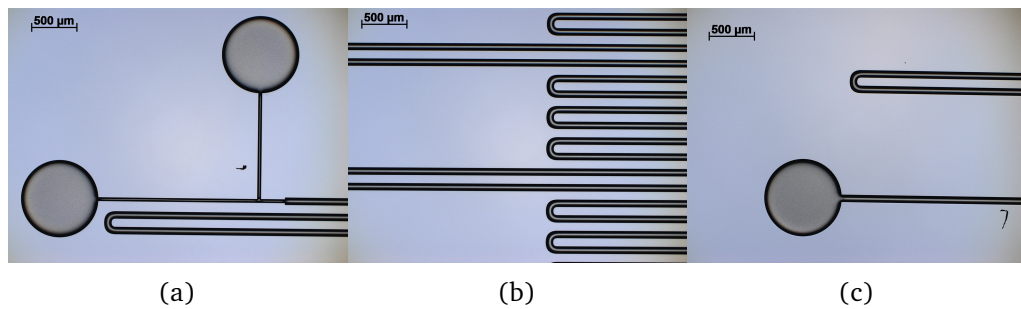


Figure 4.11: Microscope pictures of a chip wafer in 2.5X magnification. T-junction and inlets (a), channels of the extension region (b), outlet (c).

The channels are well-formed and highly uniform. The channel widths were estimated optically to be between 149 and 151  $\mu\text{m}$ . Later, the cross-section of a silicon chip was investigated with an optical microscope using 5x magnification. The resulting pictures can be seen in Figure 4.12.

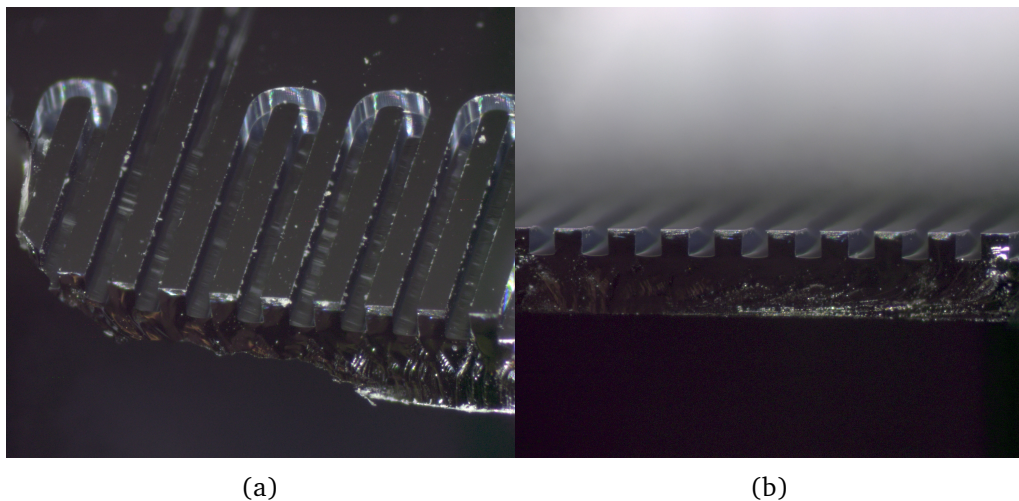


Figure 4.12: Microscope pictures of the channels of a silicon chip in 5X magnification. T-junction and inlets (a), channels of the extension region (b).

It can be observed in 4.12b that the channel walls are uniformly vertical, while the channel bottoms are slightly bowed, which is expected as the etching step of the Bosch process is isotropic. In 4.12a at the turns of the channels, we can also notice faint scalloping, also a characteristic of the Bosch process.

#### 4.3.1 Moulded PDMS Chips

Into the mould wafers the negative of the channels was etched. These were then used to cast chips out of PDMS. The resulting chips were roughly 5 mm thick and were plasmabonded to glass wafers to cap off the channels.

While the initial tests were promising, the chips showed a tendency to delaminate easily. In droplet generation tests, the chips generated droplets of uniform size and frequency, but

the droplets seemed to get stuck and fused in the first turn of the channels, as shown in Figure 4.13.



Figure 4.13: Picture showing the droplets generated on the moulded PDMS chip collecting in the first turn of the channel. The droplets are coloured with fluorescein sodium salt (NaFluo).

This has likely happened due to channels deforming. Since PDMS is a highly flexible material, placing it down on the glass plate without deforming it is close to impossible. These deformations were visible when the chip was held to the light (Figure 4.14). Because of this, the moulded chips were not investigated further. All results shown beyond this point are the results of silicon etched chips.

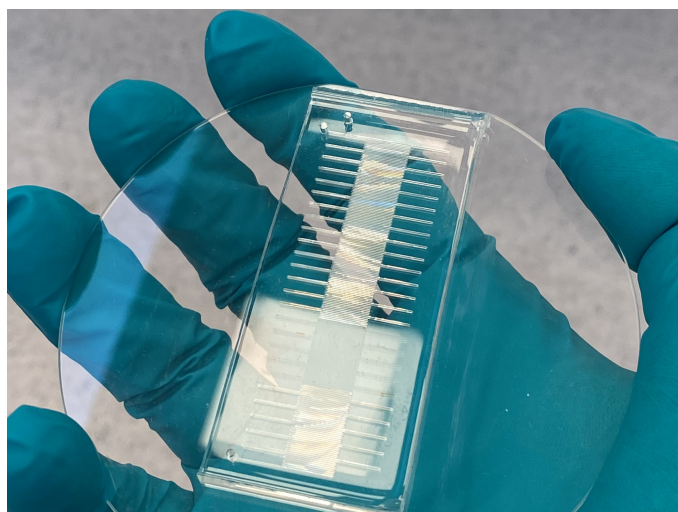


Figure 4.14: Picture showing the visible deformation of the moulded channels.

## 4.4 Qualities of the Fabricated Supporting Components

The supporting components, like the chip holder, have gone through many changes during our research. In this section, we will briefly describe the development of each component, what was tried and what was changed, and how the final versions perform.

### 4.4.1 PDMS Coverplate

Polydimethylsiloxane were prepared according to the manufacturer's instructions in a 10:1 PDMS base to curing agent ratio. To bond the PDMS to our silicon chip, three methods were investigated: plasma treatment, ozone treatment, and mechanical bonding.

Mechanically pushing the PDMS plate onto the chip resulted in fast delamination. Ozone treatment proved much more promising. The PDMS plate and the chip were treated with ozone for 30 minutes, pressed together, and then left in an 80 °C oven overnight. The resulting bond was able to withstand between 1 to 3 uses. Due to the lengthy process, a more robust bonding method was needed, which was found in plasma bonding. Plasmas-bonded chips were found to be able to withstand about 20 uses before delamination.

### 4.4.2 3D printed Chip Holder

At first, prototyping was carried out on filament 3D printed holders. Several materials were tried, including several TPU, ABS and PLA filaments. All of the resulting holders either melted or were heavily deformed due to the high temperature of the melting heater.

The solution was found in resin printing. 3D Premium's Standard Clear resin was used. While it is not graded for DNA melting temperatures, we have found it does withstand them if the chip holder's walls are sufficiently thick.

### 4.4.3 Heating System

To assess the performance of the heating system and the quality of the temperature gradient across the chip, pictures were taken with a thermal camera.

Since our chip is covered by PDMS, which blocks out infrared light, measuring its temperature directly was not possible. Empty silicon chips without PDMS were examined as well, but the surface of the chip has proven to be too reflective to measure properly. We have decided to measure the surface of the thermal clay below the chip. The system was left to equilibrate for 30 minutes with the chip on, and then the measurements were taken immediately after lifting the chip off. The measurement can be seen in Figure 4.15, showing the temperature of the denaturation zone to be 94.3 °C, the extension zone 67.5 °C and the annealing zone 48.0 °C.

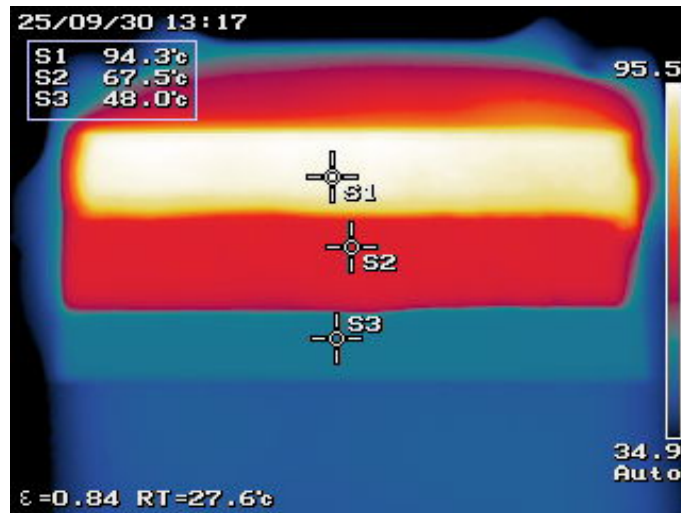


Figure 4.15: Thermal camera picture of the temperature zones of the chip. Melting zone (S1), extension zone (S2), annealing zone (S3).

Note that these values closely represent the results of our simulations. In Figure 4.16, the simulated heatmap of the chip's surface is overlaid on a thermal picture of the device. While we cannot declare for sure that these are the temperatures on the surface of the chip, due to the measurement method, we can say that the temperature gradient's profile is as expected.

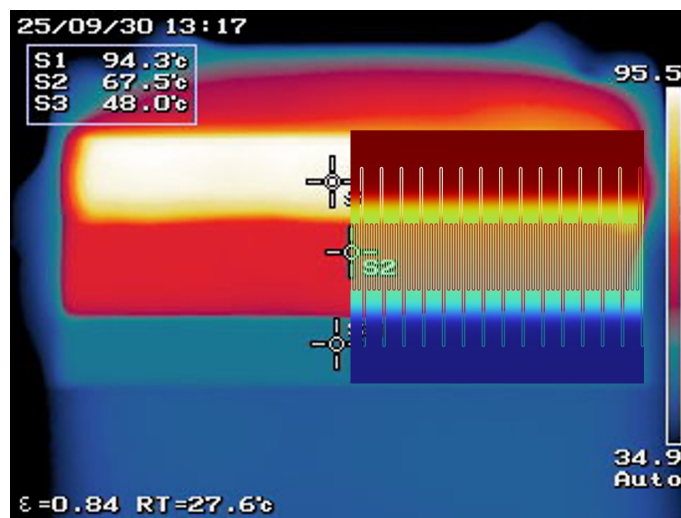


Figure 4.16: Thermal camera picture of the temperature zones of the chip with the simulated heatmap overlaid on it.

## 4.5 PCR on a Chip

The results presented were obtained on an etched silicon chip with a plasma-bonded PDMS cover plate where relevant.

### 4.5.1 Droplet Generation

Several flow rate ratios were tested for droplet generation on the integrated T-junction of the chip. Reliably stable generation was found at ratios of 1:6 dispersed phase to continuous phase flow rates. A photograph in Figure 4.17 shows the thus generated droplets in the channels of the chip.

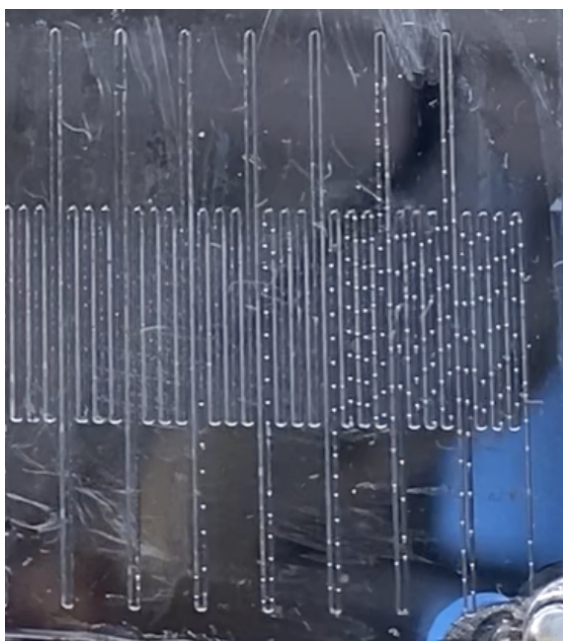


Figure 4.17: Picture of generated droplets in the channels of the chip.

The droplets are only visible on the left side of the picture. This is due to lighting and reflections. It was confirmed that the droplets are present in the whole length of the channels.

The generation rate of the droplets was measured to be 3.2 HZ. The flow rates of the dispersed and continuous phases were  $0.5 \mu\text{l}/\text{min}$  and  $3.0 \mu\text{l}/\text{min}$ , giving a total flow rate of  $3.5 \mu\text{l}/\text{min}$ . By dividing the flow rate of the dispersed phase by 60 times the generation rate, we obtain the average size of a droplet, which is  $0.002604 \mu\text{l}$ , or 2.6 nl in this case.

### 4.5.2 Polymerase Chain Reaction

The pFCPEX1D plasmid DNA was used to perform general PCRs and PCRs on a silicon microfluidic chip. Several PCR experiments were performed on the silicon chip. Only the following three PCR experiments showed notable results. The PCRs on the chip were conducted using the same parameters except for the temperature of the denaturation zone, which was varied by  $5^\circ\text{C}$  to account for the potential inaccuracy of our temperature

measurement. The temperatures were 89 °C, 94 °C, and 99 °C. The flow rates for these experiments were the same: 3  $\mu$ l/minute total. From the 1% agarose gels, it can be seen that the general PCR product is around 1000 bp. The expected fragment size for the PCR is 1077 bp. The result of the microfluidic chip, using the same PCR mixture as during the general PCR procedure, shows two DNA fragment bands on the agarose gels. One at around 4000 bp, which is the same size as the uncoiled plasmid template, and a second that is smaller than 500 bp. There were no significant differences between the three PCRs conducted on the chip (Figure 4.18a). To test whether the template DNA or other components of the PCR mixture are adsorbed in the analytical valve, an experiment was conducted. The PCR mixture was injected into the analytical valve, and after around 15 minutes of incubation, the mixture was removed. Then, the PCR mixture was run as a conventional PCR. On the 1% agarose gel, the general PCR and the PCR that was incubated in the analytical valve showed the same products (Figure 4.18b).

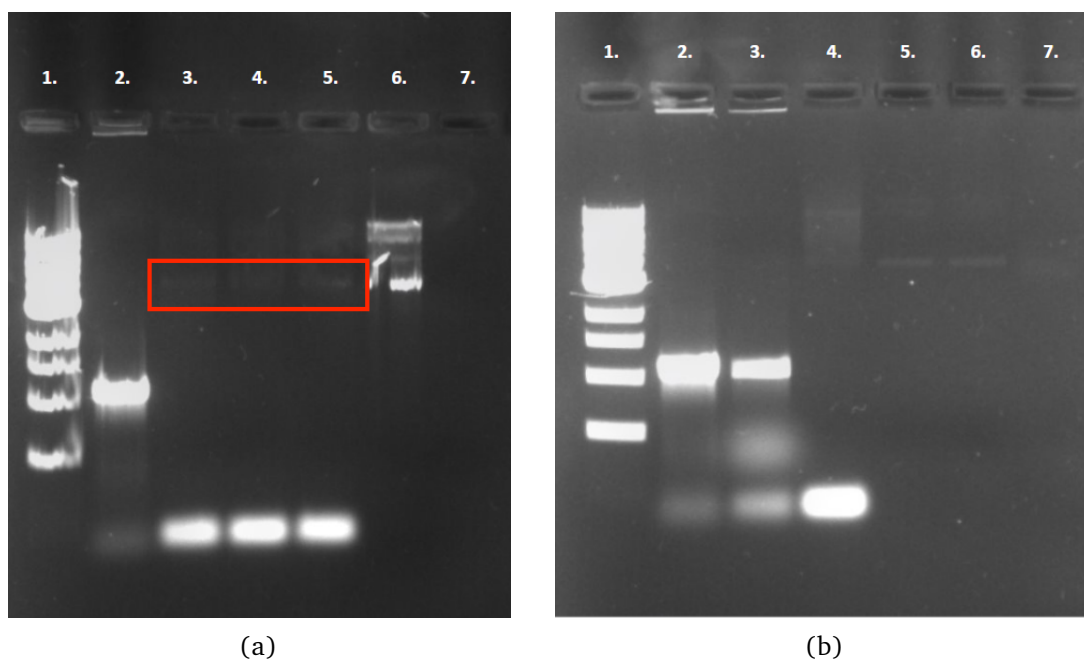


Figure 4.18: 1% agarose gel (a) showing: a 1kb DNA ladder in lane 1, general PCR product of pFCPEX1D plasmid in lane 2, PCR on a silicon chip with 94 °C in the denaturation zone in lane 3, PCR on a silicon chip with 89 °C in the denaturation zone in lane 4, PCR on a silicon chip with 99 °C in the denaturation zone in lane 5, pFCPEX1D plasmid DNA in lane 6, and water in lane 7. In lanes 4-6, the template DNA are marked with a red box for better visibility. 1% agarose gel (b) showing: A 1kb DNA ladder is in lane 1, general PCR product of pFCPEX1D plasmid in lane 2-3, PCR on a silicon chip in lane 4, pFCPEX1D plasmid DNA in lane 5-6, and HSA (10mg/ml) in lane 7. The samples contained 5  $\mu$ l with 1  $\mu$ l loading dye from New England BioLabs, and 5  $\mu$ l of 1kb DNA ladder from New England BioLabs was used.

With the appearance of the smaller fragments, a PCR experiment was conducted without template DNA to assess if the smaller products are components of the PCR mixture, specifically primers or primer dimers (Figure 4.19).

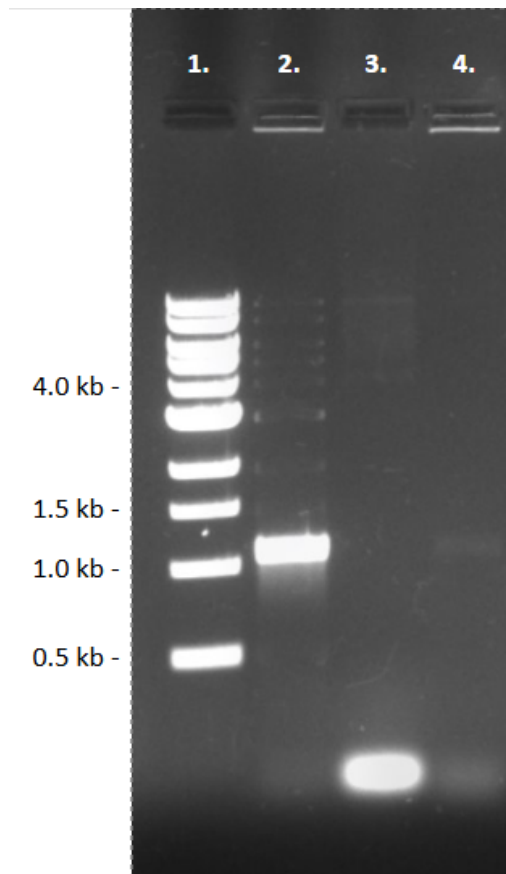


Figure 4.19: On 1% agarose gel, 1kb DNA ladder is in lane 1, general PCR product of pFCPEX1D plasmid is in lane 2, PCR on a silicon chip is in lane 3, general PCR product without template DNA is in lane 4. The samples contained 5  $\mu$ l with 1  $\mu$ l loading dye from New England BioLabs, and 5  $\mu$ l of 1kb DNA ladder from New England BioLabs was used.

To measure the smaller fragments on the previous gel pictures, a 1% agarose gel was run with a 100 bp ladder. A general PCR sample and the general PCR without template DNA were run alongside the three samples of the PCR experiment on the microfluidic chip. It can be seen that the smaller fragments' sizes are a maximum of 100 bp (Figure 4.20).

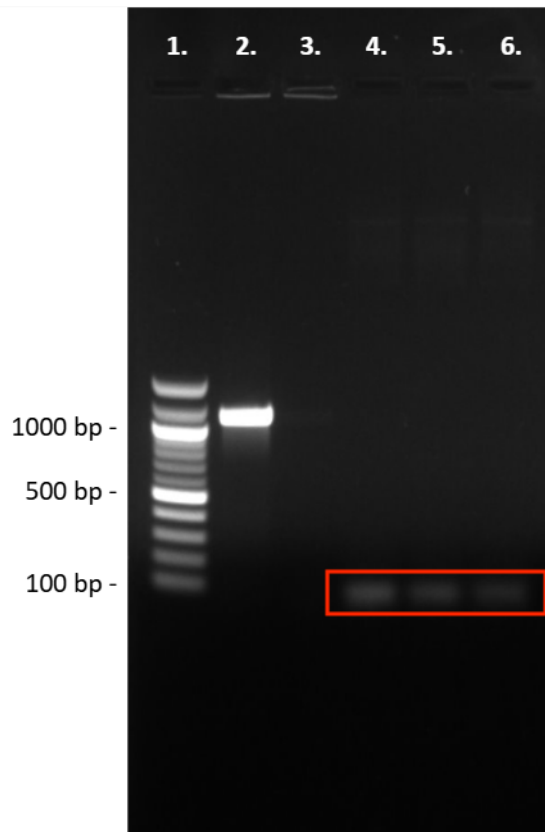


Figure 4.20: On the 1% agarose gel a 100 bp DNA ladder is in lane 1, general PCR product of pFCPEX1D plasmid is in lane 2, general PCR product without template DNA is in lane 3, PCR on a silicon chip with 99 °C in the denaturation zone is in lane 4, PCR on a silicon chip with 89 °C in the denaturation zone is in lane 5, and PCR on a silicon chip with 94 °C in the denaturation zone is in lane 6. The samples contained 5  $\mu$ l with 1  $\mu$ l loading dye from New England BioLabs, and 5  $\mu$ l of 100 bp DNA ladder from New England BioLabs was used. In lanes 4-6, the PCR on a chip products are marked with a red box for better visibility.

# Discussion 5

---

## 5.1 PCR on a Chip

Peculiar products were observed when conducting PCR on our chip (Figure 4.18a). To assess whether these results are due to adsorption in our system, an experiment was conducted. Since the chip could not be heated to stop potential amplification from happening, and since the paraffin oil used is too viscous at room temperature, the sample could not be incubated in our chip. The sample was kept for 15 minutes in the analytical valve instead, as we had suspected contamination of the component.

Figure 4.18b's lane 3 suggests a slight inhibition of the product after incubation in the valve. A new, spread-out band is produced as well. In our experience, this is characteristic of NaFluo in the sample. Fluorescein Sodium Salt is used by our peers with whom we share the setup. It was found that NaFluo has an inhibitory effect on PCR, which could explain the results. After these findings, the valve was disassembled and thoroughly cleaned.

As the products of the PCR on a chip are in the primer fragment size range, it was investigated whether these are primer-dimers or not. Das *et al.* [39] found that stable primer-dimer formation only occurs in the presence of DNA polymerase, so a PCR mixture was prepared with all of its components, except for the DNA template, and then run on a conventional thermocycler to produce as many primer-dimers as possible.

The results in Figure 4.20 suggest the possibility that the PCR on a chip products are not primer-dimers. In lane 3, we can see the primer-dimer only experiment. The product's band intensity is much lower than the band intensity of the PCR on a chip samples, which could point to some kind of amplified product instead of primer-dimers. It is possible that the sample's time spent in the extension zone on the chip is too short, creating asymmetric products by melting mid extension.

### 5.1.1 Future PCR on a chip experiments

To confirm if these products are primer-dimers or some other products, the following experiments could be conducted. If the products are the result of incomplete extension, lowering the total flow rate of the device should result in larger products. Since the extension rate is possibly very low, increasing the concentration of Taq polymerase could also help [16].

If the products are indeed primer-dimers, it is possible that the reason for their presence is the chip's melting temperature being too low. If the denaturation temperature is sufficiently

low, so that the template DNA does not melt in the denaturation zone, only primer-dimers could be present in the product. For this to happen, the temperature would have to be much lower than expected, as template DNA does melt even at lower temperatures, just in smaller quantities, giving fewer products. Experiments with much higher denaturation temperature settings could be carried out to confirm this.

## 5.2 Heating System — Problems and Improvements

The temperature measurements of the heating systems, specifically the melting heater, are uncertain for several reasons. Firstly, since the heating setup is shared by two groups, fixing the platinum sensors in place is not an option. This results in the temperature controllers not being properly calibrated, and the measurements differing by a few degrees between uses. To combat this, we used the thermal camera before each use to set the temperatures.

Secondly, because we cannot measure the temperature of our chip directly, it is hard to say its value. We have determined the temperature by measuring the surface of the thermal clay immediately after removing the chip. The temperature loss between the measurement and the removal is likely not negligible, which is likely why the extension zone's copper block is a bit cooler than expected.

The temperature of the melting heater also fluctuated a lot during our test, up to 5-6 °C at times. This is problematic, as 94 °C is needed to initially denature the template DNA, and while Taq polymerase is thermostable, its half-life decreases rapidly above 95 °C. At 97.5 °C, it is only 5-6 minutes [40].

Both accurate temperature measurement and heating are aspects to be improved upon. A thin-film platinum sensor could be integrated into the chip by a combination of lithography, chemical etching, and sputtering [41]. This would result in a highly accurate temperature measurement method. The drawback is its complexity and cost if integrated into each chip.

Fukuba *et al.* [42] suggests separating the microfluidics and the heating into a PCR chip and a temperature control chip. The temperature control chip consists of integrated platinum sensors and six indium tin oxide (ITO) heaters. The integration of ITO heaters would allow for a smaller footprint and tighter control, but due to the large temperature difference between the edges of the chip, overheating could prove problematic.

## 5.3 Droplet Generation and Flow

Our microfluidic PCR chip with integrated droplet generation has shown great promise in producing stable and uniform droplets. Due to clogging and delamination at the dispersed phase inlet, the experiments were halted. While the average volume of the droplets was measured using their generation rate and the flow rate of the dispersed phase, microscope pictures are required to determine the uniformity and size distribution of these droplets. NaFluo could be used to make the droplets more visible.

A common problem with the design presented in this paper is delamination near the input of the continuous phase due to the inlet and the first turn of the annealing zone being too close together. In Figure 5.1, this problematic area is marked by a red circle.

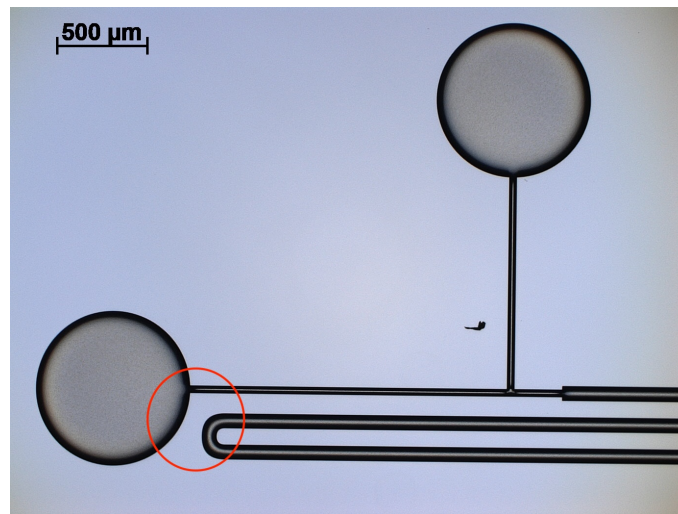


Figure 5.1: Picture of an input area of a PCR chip. The inlet of the continuous phase and the first turn of the annealing zone are marked by a red circle.

Due to this geometry, chips often had to be redone when puncturing the inlets in the PDMS plate, and in almost all cases, this was the first point of failure of the device. When delamination occurs in this area, the number of cycles is reduced by one, since the first denaturation zone is bypassed. Droplet generation also becomes unreliable as the T-junction is no longer in use, resulting in a large size distribution of droplets and plugs.

While stable droplets were generated, due to possibly low extension rates, the total flow rate might need to be slowed down. Insufficient flow rate could cause the droplets to fuse. To prevent this, future designs would greatly benefit from longer channels in the extension zone. Widening the chip and the centre copper block would allow us to greatly increase the volume of the extension zone. This would have several benefits. Faster flow rates would be achievable, which would result in better droplet stability and ultimately faster thermal cycling.

## 5.4 Optimisations and Possible Improvements

There are still several optimisation and improvement options that are outside the scope of this project. Here are some notable examples listed.

### 5.4.1 Dead Volume

Dead volume is defined as the volume of the microfluidic system that is not essential for its function and thus could be eliminated. In our system, dead volume is present in several locations. Firstly, the inlets on the chip are on the annealing side. This was done for convenience's sake and for easier handling, but is otherwise completely unnecessary and contributes roughly  $0.68 \mu\text{l}$  of dead volume.

The biggest contributor to dead volume is the tubing of the injection system. To combat this, the oil phases were first manually pushed to the end of the tubing, and only then were connected to the chip. This is fine in research, but for commercial applications, it is essential to eliminate these.

#### 5.4.2 BSA and Surfactant Concentration

In our experiments, serum albumin was added to the PCE mixture in a concentration of 10 mg/ml, and Triton X-100 in 1% to the paraffin oil. The function of the non-ionic surfactant is to stabilise the droplets and to slightly increase the extension rate of Taq polymerase. Similarly, BSA helps with droplet stabilisation, increases the specificity of the PCR, and prevents adsorption to the surfaces of the device. It is especially important, as adsorption could occur in the valve and the tubing before the chip, where the sample is not in droplet form and can interact with surfaces.

Triton X-100 concentration was derived from droplet PCR kit recipes, while BSA concentration is based on the work of Christensen *et al.* [17]. Both these values are meant as starting points for further optimisation. By running several samples with varying concentrations, one could optimise them by comparing the relative band intensities of each sample.

#### 5.4.3 Extension Rate Optimization

Several factors affect the extension rate of Taq polymerase [16]. In our case, its concentration and the temperature of the chip require further optimisation. Due to adsorption, Taq polymerase concentration could decrease; increasing its initial concentration could improve results.

Since the temperature of our chip is uncertain, the extension region might not be in the optimal temperature range of 70 to 75 °C. Further experiments with varying temperatures are required.

Another possibility of improving the extension rate is the use of T<sub>m</sub> repressors, such as dimethyl sulfoxide (DMSO) [16]. DMSO has been shown to disrupt secondary structure formation in the DNA template and to increase the extension rate of Taq polymerase. Reducing primer T<sub>m</sub> also increases the specificity of the reaction, which might be beneficial for most droplet PCR purposes, such as diagnostics.

# Conclusion 6

---

In this paper, the design and fabrication of a continuous-flow fixed-loop droplet-based PCR on a chip with integrated droplet generation were investigated. Conventional PCR methods are held back by their large thermal mass, which makes the process lengthy. Microfluidic lab-on-a-chip approaches have the potential for faster thermal cycling and reduced consumption of reagents. On the other hand, these methods are easily inhibited by the adsorption of PCR components due to their large surface-to-volume ratios. Droplet-based PCR circumvents this by eliminating the contact between the sample and the device's surface.

Three fabrication methods were explored, including laser ablation, dry etching, and polymer casting. Etching microfluidic channels into silicon was found to be the most robust solution. The chip was fabricated using the Bosch method, with a T-junction integrated into the design. The channels of the chip were capped off with a PDMS coverplate using plasma-bonding.

The heat distribution of the device was first simulated in COMSOL. Stable temperature regions were generated using one resistive heater and one Peltier heater on two edges of the chip. Three copper blocks were used to further define the regions.

The device is capable of generating stable and uniform droplets. The PCR product of the chip was found to be shorter than expected. These are possibly asymmetric products that are being generated due to not enough time spent in the extension region of the chip. Slower flow-rates and increased denaturation temperature are to be further examined.

# Bibliography

---

- [1] F. SANGER, S. NICKLEN, and A. R. COULSON, "Dna sequencing with chain-terminating inhibitors," *Proc. Natl Acad. Sci.*, 1977.
- [2] K. Mullis *et al.*, "Specific enzymatic amplification of dna in vitro: The polymerase chain reaction," *Cold Spring Harbor Symposia on Quantitative Biology*, 1986.
- [3] S. RK *et al.*, "Primer-directed enzymatic amplification of dna with a thermostable dna polymerase," *Science*, 1988.
- [4] H. Zhu *et al.*, "Pcr past, present and future," *BioTechniques*, 2020.
- [5] G. R. T. M. J. McPherson P. Quirke, Ed., *PCR: a practical approach*. English. Oxford: IRL Press at Oxford University Press, 1991, xxi + 253 pp. ISBN: 0-19-963226-X 0-19-963196-4 9780199632268 9780199632268.
- [6] C. T. Wittwer and M. G. Herrmann, "Rapid thermal cycling and pcr kinetics," *PCR Applications*, 1999.
- [7] Y. Zhang and P. Ozdemir, "Microfluidic dna amplification—a review," *Analytica Chimica Acta*, 2009.
- [8] H. Nakano *et al.*, "High speed polymerase chain reaction in constant flow," *Bioscience, Biotechnology, and Biochemistry*, 1994.
- [9] N. A. Friedman and D. R. Meldrum, "Capillary tube resistive thermal cycling," *Analytical Chemistry*, 1998.
- [10] C. J. Bruckner-Lea *et al.*, "Renewable microcolumns for automated dna purification and flow-through amplification: From sediment samples through polymerase chain reaction," *Analytica Chimica Acta*, 2002.
- [11] P. Belgrader *et al.*, "A reusable flow-through polymerase chain reaction instrument for the continuous monitoring of infectious biological agents," *Analytical Chemistry*, 2003.
- [12] M. U. Kopp *et al.*, "Chemical amplification: Continuous-flow pcr on a chip," *Science*, 1998.
- [13] A. Gonzalez *et al.*, "Interaction of quantitative PCR components with polymeric surfaces," *Biomed Microdevices*, 2007.
- [14] T. B. Christensen *et al.*, "PCR biocompatibility of lab-on-a-chip and mems materials," *Journal of Micromechanics and Microengineering*, 2007.
- [15] R. Kodzius *et al.*, "Inhibitory effect of common microfluidic materials on PCR outcome," *Sensors and Actuators B: Chemical*, 2012.
- [16] J. L. Montgomery and C. T. Wittwer, "Influence of PCR reagents on dna polymerase extension rates measured on real-time PCR instruments," *Clinical Chemistry*, 2014.

- [17] T. B. Christensen *et al.*, “Multiplex polymerase chain reaction (PCR) on a su-8 chip,” *Microelectronic Engineering*, 2008.
- [18] S. Mohr *et al.*, “Numerical and experimental study of a droplet-based pcr chip,” *Microfluid Nanofluid*, 2007.
- [19] V. Taly *et al.*, “Droplets as microreactors for high-throughput biology,” *ChemBioChem*, 2007.
- [20] L. Garibyan and N. Avashia, “Polymerase chain reaction,” *Journal of Investigative Dermatology*, 2013.
- [21] P. Wilding, M. A. Shoffner, and L. J. Kricka, “PCR in a silicon microstructure,” *Clinical Chemistry*, 1994.
- [22] P. Belgrader *et al.*, “PCR detection of bacteria in seven minutes,” *Science*, 1999.
- [23] M. Bu *et al.*, “Design and theoretical evaluation of a novel microfluidic device to be used for PCR,” *Journal of Micromechanics and Microengineering*, 2003.
- [24] J. West *et al.*, “Application of magnetohydrodynamic actuation to continuous flow chemistry,” *Lab on a Chip*, 2002.
- [25] P. O. Yonghao Zhang, “Microfluidic dna amplification—a review,” *Analytica Chimica Acta*, vol. 638, no. 2, pp. 115–125, 2009.
- [26] L. B. Neves *et al.*, “A review of methods to modify the pdms surface wettability and their applications,” *Micromachines*, 2024.
- [27] D. Xu, W. Zhang, H. Li, N. Li, and J.-M. Lin, “Advances in droplet digital polymerase chain reaction on microfluidic chips,” *Royal Society of Chemistry*, 2023.
- [28] Z. Zhu, G. Jenkins, W. Zhang, and et al, “Single-molecule emulsion pcr in microfluidic droplets,” *Analytical and Bioanalytical Science*, 2012.
- [29] T. Thorsen, R. W. Roberts, F. H. Arnold, and S. R. Quake, “Dynamic pattern formation in a vesicle-generating microfluidic device,” *Physical Review Letters*, 2001.
- [30] J. Souk, S. Morozumi, F.-C. Luo, and I. Bita, *Photolithography*, 1st ed. Hoboken, NJ : John Wiley & Sons, 2018, ISBN: 1-119-16134-7.
- [31] L.-C. Xu and C. Siedlecki, “4.18 surface texturing and control of bacterial adhesion,” in *Comprehensive Biomaterials II*, P. Ducheyne, Ed., Oxford: Elsevier, 2017, pp. 303–320, ISBN: 978-0-08-100692-4.
- [32] S. Franssila, “Optical lithography,” in *Introduction to Microfabrication*. John Wiley Sons, Ltd, 2010, ch. 9, pp. 103–113. DOI: <https://doi.org/10.1002/9781119990413.ch9>.
- [33] K. Nojiri, *Dry Etching Technology for Semiconductors*. Springer, 2012.
- [34] SAMCO. “Part 2 – what is the bosch process (deep reactive ion etching)?” (), Available: <https://www.samcointl.com/news-events/tutorials/what-is-the-bosch-process/>.
- [35] C. Jiu-Sheng and J. Jia-Huan, “Droplet microfluidic technology: Mirodroplets formation and manipulation,” *CHINESE JOURNAL OF ANALYTICAL CHEMISTRY*, 2012.

- 
- [36] DTU Nanolab. "DRIE-Pegasus/processA." (2025), Available: [https://labadviser.nanolab.dtu.dk/index.php?title=Specific\\_Process\\_Knowledge/Etch/DRIE-Pegasus/processA](https://labadviser.nanolab.dtu.dk/index.php?title=Specific_Process_Knowledge/Etch/DRIE-Pegasus/processA).
- [37] COMSOL Multiphysics®. (v. 6.3.), Available: [www.comsol.com](http://www.comsol.com).
- [38] D. Y. Lando *et al.*, "Determination of melting temperature and temperature melting range for dna with multi-peak differential melting curves," *Analytical Biochemistry*, 2015.
- [39] S. Das *et al.*, "Studies on primer-dimer formation in polymerase chain reaction (pcr)," *Biotechnology Techniques*, 1999.
- [40] E. V. Pelt-Verkuil *et al.*, "Principles and technical aspects of pcr amplification," *Springer*, 2008.
- [41] J. D. Wrbanek and K. L. Laster, "Preparation and analysis of platinum thin films for high temperature sensor applications," *NASA*, 2005.
- [42] T. Fukuba *et al.*, "Microfabricated flow-through device for dna amplification—towards in situ gene analysis," *Chemical Engineering Journal*, 2004.

## **.1 Appendix A**

### **.2 Method Protocols**

#### **.2.1 UV Lithography**

The protocol for UV lithography can be found in the following web page:

[https://labadviser.nanolab.dtu.dk/index.php?title=Specific\\_Process\\_Knowledge/Lithography/UVLithography](https://labadviser.nanolab.dtu.dk/index.php?title=Specific_Process_Knowledge/Lithography/UVLithography)

The protocol for pretreatment can be found in the following web page:

[https://labadviser.nanolab.dtu.dk/index.php?title=Specific\\_Process\\_Knowledge/Lithography/Pretreatment#HMDS](https://labadviser.nanolab.dtu.dk/index.php?title=Specific_Process_Knowledge/Lithography/Pretreatment#HMDS)

The protocol for coating can be found in the following web page:

[https://labadviser.nanolab.dtu.dk/index.php?title=Specific\\_Process\\_Knowledge/Lithography/Coaters#Spin\\_Coater:\\_Gamma\\_UV](https://labadviser.nanolab.dtu.dk/index.php?title=Specific_Process_Knowledge/Lithography/Coaters#Spin_Coater:_Gamma_UV)

The protocol for exposure can be found in the following web page:

[https://labadviser.nanolab.dtu.dk/index.php?title=Specific\\_Process\\_Knowledge/Lithography/UVExposure#Aligner:\\_Maskless\\_02](https://labadviser.nanolab.dtu.dk/index.php?title=Specific_Process_Knowledge/Lithography/UVExposure#Aligner:_Maskless_02)

The protocol for development can be found in the following web page:

[https://labadviser.nanolab.dtu.dk/index.php?title=Specific\\_Process\\_Knowledge/Lithography/Development#Developer\\_TMAH\\_UV-lithography](https://labadviser.nanolab.dtu.dk/index.php?title=Specific_Process_Knowledge/Lithography/Development#Developer_TMAH_UV-lithography)

#### **.2.2 Dry Etch**

The protocol for dry etch can be found in the following web page:

[https://labadviser.nanolab.dtu.dk/index.php?title=Specific\\_Process\\_Knowledge/Etch/DRIE-Pegasus/processA](https://labadviser.nanolab.dtu.dk/index.php?title=Specific_Process_Knowledge/Etch/DRIE-Pegasus/processA)

#### **.2.3 Post Processing**

The protocol for antistiction coating can be found in the following web page:

[https://labadviser.nanolab.dtu.dk/index.php?title=Specific\\_Process\\_Knowledge/Thin\\_film\\_deposition/Antistiction\\_Coating#The\\_STAMP\\_recipe](https://labadviser.nanolab.dtu.dk/index.php?title=Specific_Process_Knowledge/Thin_film_deposition/Antistiction_Coating#The_STAMP_recipe)

#### **.2.4 GeneJET Plasmid Miniprep Kit**

This protocol is used for plasmid isolation from cells. The cell tube has already been incubated overnight at 37° C. The contents of the tube are transferred to a 15 ml tube with

a screw lid for easier centrifugation and centrifuged at 6° C at 6.000 rpm for 7 minutes. The supernatant is discarded, leaving the cell pellet facing upward in the tube.

Step 1: 250  $\mu$ l Resuspension Solution is added into the 15 ml tube with pellet and vortex. The supernatant is transferred into an Eppendorf tube and 250  $\mu$ l Lysis solution is added to the tube and inverted 6 times. 350  $\mu$ l Neutralization Solution is added and again inverted 6 times. This is centrifuged for 10 minutes at 12.000 rpm.

Step 2: Transfer only the supernatant to the Thermo Scientific GeneJET spin Column (as pellet fragments may clog up the filter). This is done with a pipet. The liquid is centrifuged for 1 minute at 12.000 rcf through the GeneJET spin Column filter and the eluate is discarded. If there is not enough room for all the eluate to flow through, the eluate is discarded and the tube is centrifuged again.

Step 3: Add 500  $\mu$ l of Wash Solution and centrifuge for 1 minute at 12.000 rcf. Discard the flow through. This is repeated. Centrifuge the empty column tube for 1 minute at 12.000 rcf.

Step 4: Transfer the column into a new tube. Add 50  $\mu$ l Elution Buffer to the column and incubate for 2 minutes Centrifuge for 2 minutes (the Eppendorf lid can be orientated so it matches the counterweight) at 12.000 rcf. The flowthrough is collected in a new Eppendorf tube.